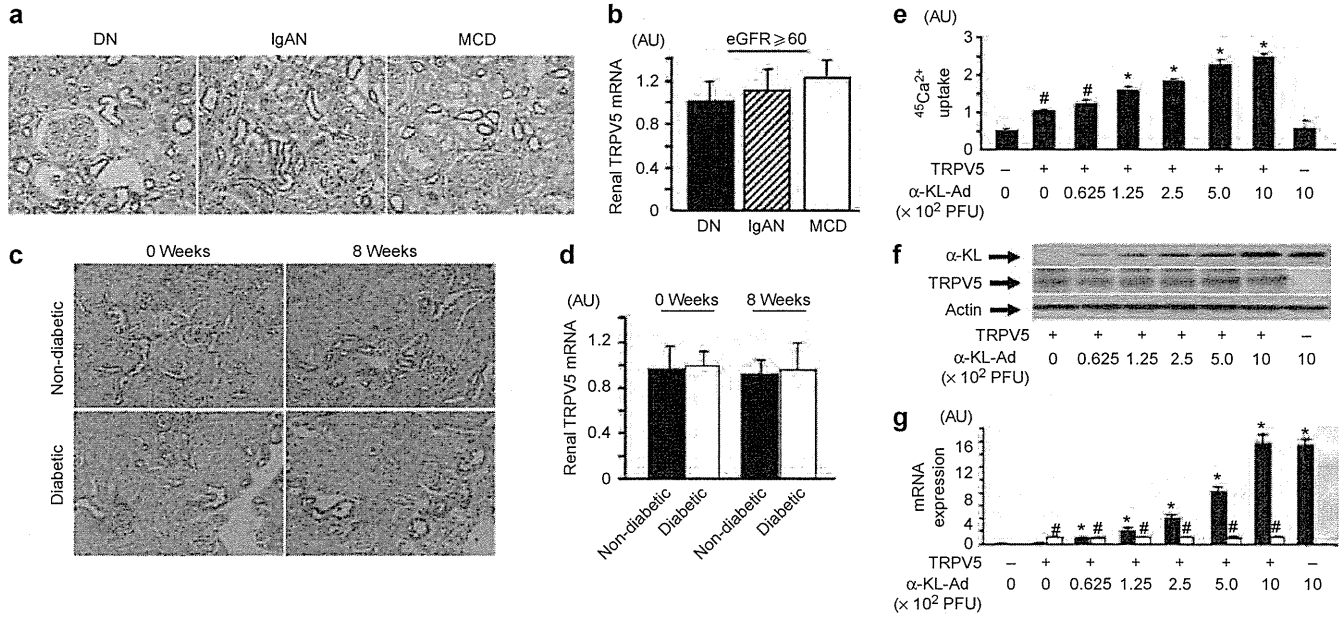

Figure 7 | The effect of α-KL expression levels on the activity of transient receptor potential vanilloid calcium channel subtype 5 (TRPV5). (**a**) Representative immunoperoxidase staining for TRPV5 in renal biopsy sections from human patients with diabetic nephropathy (DN), IgA nephropathy (IgAN), and minimal change disease (MCD). (**b**) Renal TRPV5 mRNA expression levels in DN (black bars), IgAN (striped bars), and MCD (white bars). (**c**) Representative immunoperoxidase staining for TRPV5 in kidney specimens from the indicated mice. (**d**) Renal TRPV5 mRNA expression levels in STZ diabetic (black bars) and nondiabetic (white bars) mice. (**e**) $^{45}Ca^{2+}$ uptake in HEK293 cells transfected with adenovirus carrying the *α-KL* gene (α-KL-Ad) or *Lac Z* gene as control, at the indicated doses, with or without TRPV5 expression. (**f**) Western blotting and (**g**) mRNA expression levels of α-KL (black bars) and TRPV5 (white bars) in the indicated HEK293 cells. Data are shown as means ± s.e.m. for each group. Original magnification, × 100. Student's *t*-test was used to compare groups. $^{\#}P<0.05$, vs. HEK293 cells without TRPV5 and α-KL gene transfected; $^{*}P<0.05$, vs. HEK293 cells transfected with TRPV5 and Lac Z.

α-$KL^{+/+}$ mice within 2 weeks after the establishment of diabetes mellitus, even when DN-related further decline of α-KL expression was not detected (Figure 6). Therefore, the increased UCa/UCr levels in the diabetic patients and mouse model of diabetes result from not only some diabetes-related changes such as glomerular hyperfiltration of calcium but also the 50% reduction in renal α-KL mRNA expression. Thus, hypercalciuria in the early stages of DN is at least partly due to α-KL loss in DCT.

Recently, evidence has accumulated that TRPV5 and Na^+/K^+-ATPase were carriers to mediate the activity of α-KL on calcium excretion in the DCTs.[14,18,24] Our *in vitro* analyses showed that, in HEK293 cells transfected with both TRPV5 and α-KL, calcium uptake was significantly increased in proportion to the α-KL expression, indicating that the reduction of α-KL expression may be related to a reduced abosorption of calcium via TRPV5 channels in the DCTs. This effect could reduce the capacity for calcium reabsorption in the DCTs to a level insufficient to meet the demand of the glomerular hyperfiltrated calcium in DN, which would in turn lead to more increasing urinary calcium excretion as α-KL expression levels decline. However, the other molecules including Na^+/K^+-ATPase may mediate the activity of α-KL on calcium excretion in the kidney, and further studies will be needed to more precisely clarify these underlying mechanism.

In conclusion, α-KL expression levels in the DCTs are decreased in the early stages of DN, which may affect urinary excretion of calcium in early DN.

MATERIALS AND METHODS

Study population

This study evaluated 74 patients with DN who manifested microalbuminuria, macroalbuminuria, and/or overt proteinuria, 90 patients diagnosed with IgAN by renal biopsy, and 26 patients with MCD. Spot urine and serum samples were collected between 0600 and 1000 h after a 10-h overnight fast. Serum levels of total protein, albumin, creatinine, calcium, inorganic phosphate, and glucose, as well as urinary levels of protein, creatinine, calcium, and inorganic phosphate, were measured in all patients. Serum $1,25(OH)_2$ vitamin D_3 levels were measured by radioimmunoassay, and serum i-PTH levels were measured by ECLIA (SRL, Tokyo, Japan). Serum fibroblast growth factor 23 concentrations were measured by using an ELISA kit (Kainos laboratories, Tokyo, Japan). eGFR was calculated by the creatinine-based Modification of Diet in Renal Disease Study equation.[25] Patient characteristics are listed in Table 1. In this study population, we evaluate renal α-KL expression levels in 31 patients with DN who had undergone renal biopsy, 31 patients with IgAN, and 7 patients with MCD. Renal biopsy had been performed in patients, whose amount of urinary protein was over 0.5 g/day. The patient characteristics of this subset used to evaluate renal α-KL expression are listed in Supplementary Table online. All clinical study protocols were approved by our institutional ethics committee (No. 2002-009, Nara Medical University Ethics

Committee). Written informed consent was obtained in all cases from either the patient or his or her family members.

Animal studies

C57BL/6 mice, originally obtained from Japan Clea (Tokyo, Japan), and α-KL$^{+/-}$ mice[15] were housed under specific pathogen-free conditions in the Animal Research Institute of Nara Medical University. Diabetes was induced in both adult male C57BL/6 mice and α-KL$^{+/-}$ mice at 8 weeks of age by intraperitoneal injections of STZ (200 mg/kg) as previously reported.[26] Mice were individually housed in metabolic cages to obtain 24-h urine collections before killing. Commercial kits were used to measure concentrations of urine creatinine and calcium (Creatinine-Test and Calcium E-Test Wako, Wako, Wako Pure Chemical Industries, Osaka, Japan), as well as albumin (Albuwell M, Exocell, Philadelphia, PA). All procedures involving mice were performed in accordance with the National Institutes of Health guidelines for the care and use of live animals and were approved by the Nara Medical University Animal Care Committee.

Immunohistochemical studies

α-KL was immunohistochemically labeled using KM2076 antibody (1:50 dilution; a kind gift of Kyowa Hakko Kogyo);[27] human type I collagen was labeled using mouse anti-human collagen type I monoclonal antibodies (1:500 dilution; MP Biomedicals, LLC, Solon, OH); TRPV5 was labeled using rabbit anti-rat TRPV5 polyclonal antibodies (1:100 dilution; Alpha Diagnostic International, San Antonio, TX) in sections from human renal biopsy specimens and murine kidneys. Human CD31, a marker of PTCs, was labeled using mouse anti-human CD31 monoclonal antibodies (1:100 dilution; Dako, Glostrup, Denmark). After primary antibody staining, labeling was visualized using a Dako Envison Kit. The number of CD31-positive PTCs within the confines of each of 10 random fields (delineated by a 1-cm^2 ocular grid viewed at × 100 magnification) was expressed as a mean per field. We also evaluated the mean percentages of each of 10 random fields positive for type I collagen by using an auto-analyzer.

DNA constructs

The coding sequence of wild-type TRPV5 was amplified from mouse (strain C57BL/6) kidney cDNA and cloned into the pcDNA3 vector (TRPV5-pcDNA3 vector). The coding sequence of wild-type α-KL was amplified from mouse (strain C57BL/6) kidney cDNA, and recombinant adenoviral vector carrying *α-KL* gene (adeno-α-KL) was constructed using the Adeno-X expression system according to the manufacturer's protocol (Clontech laboratories, Mountain View, CA). All constructs were verified by DNA sequence analysis.

Cell transfection and $^{45}Ca^{2+}$ uptake assay

HEK293 cells were transfected with TRPV5-pcDNA3 vector using the FuGENE HD transfection reagent according to the manufacturer's protocol (Roche, Mannheim, Germany), and cultured in Dulbecco's modified Eagle's medium containing 10% fetal bovine serum, and infected with adeno-α-KL and the control adeno-Lac Z, respectively, in a six-well plate. Two days after transfection, $^{45}Ca^{2+}$ (1 uCi/ml) uptake was performed as described previously.[28,29]

Western blotting

Kidney and cell lysates were prepared using lysis buffer, and western blot analysis was performed as previously reported,[27,29] using specific antibodies, including monoclonal rat antibody for α-KL protein (KM2076)[27] (1:500 dilution) and polyclonal rabbit antibody for TRPV5 protein (1:100; Alpha Diagnostic International).

RNA extraction, reverse transcription, and real-time RT-PCR

Total cellular RNA was extracted from human frozen renal biopsy specimens, murine renal cortex, or HEK293 cells, and first-strand cDNA was constructed as previously described.[30,31] For real-time PCR, 1 μl of each first-strand reaction product was amplified with appropriate primers and the corresponding fluorescent probes for human and murine α-KL (assay IDs: Hs00183100_m1, Mm00502002_m1) and TRPV5 (assay IDs: Hs00219765_m1, Mm01166029_m1), human β-actin (assay ID: Hs00242273_m1), or murine glyceraldehydes-3-phosphate dehydrogenase (assay ID: Mm99999915_m1). These probes were designed by the Applied Biosystems 'Assay-on-Demand' service (Foster City, CA). The ratios of human α-KL/β-actin mRNA, human TRPV5/β-actin mRNA, murine α-KL/glyceraldehydes-3-phosphate dehydrogenase mRNA, and murine TRPV5/glyceraldehydes-3-phosphate dehydrogenase mRNA were calculated for each sample.

Statistical analysis

Statistical analyses were performed with the StatView 5.0 software (SAS Institute, Cary, NC). Numerical results were expressed as means ± s.d. Student's *t*-test was used for normally distributed variables. To compare groups, we used a one-way analysis of variance, followed by *post-hoc t*-test with Fisher-Protected Least Significant Differences adjustment. For variables with a skewed distribution, we used a Kruskal–Wallis analysis of variance by ranks with Bonferroni adjustment. The Pearson correlation coefficient was used to assess the relationships between renal α-KL mRNA expression levels and clinical and pathological parameters. Multiple regression analysis was performed to assess the combined influence of clinical variables on UCa/UCr among all patients with DN, IgAN, and MCD, who had undergone renal biopsy. Independent variables included levels of renal α-KL expression, serum $1,25(OH)_2$ vitamin D_3, serum i-PTH, corrected serum calcium, as well as eGFR and age. *P*-values less than 0.05 were considered to be significant.

DISCLOSURE

All the authors declared no competing interests.

ACKNOWLEDGMENTS

This work was supported in part by a research grant from the Ministry of Education and Science of Japan. We are indebted to Miss Aya Asano and Mrs Miyako Sakaida of Nara Medical University for their excellent technical assistance.

SUPPLEMENTARY MATERIAL

Figure S1. Time course of urinary albumin to creatinine ratios (UACR) in diabetic (closed circles) and nondiabetic (open circles) mice.

Figure S2. Representative features of STZ-induced diabetic (a, b, c) and nondiabetic (d, e, f) mouse kidneys (periodic acid–methenamine–silver stain) at 0 weeks (a, d), 4 weeks (b, e), and 8 weeks (c, f) after the establishment of diabetes.

Table S1. Clinical characteristics of patients for renal α-KL expression analysis.

Supplementary material is linked to the online version of the paper at http://www.nature.com/ki

REFERENCES

1. Raskin P, Stevenson MR, Barilla DE *et al.* The hypercalciuria of diabetes mellitus: its amelioration with insulin. *Clin Endocrinol (Oxf)* 1978; **9**: 329–335.
2. Anwana AB, Garland HO. Renal calcium and magnesium handling in experimental diabetes mellitus in the rat. *Acta Endocrinol (Copenh)* 1990; **122**: 479–486.
3. Lee CT, Lien YH, Lai LW *et al.* Increased renal calcium and magnesium transporter abundance in streptozotocin-induced diabetes mellitus. *Kidney Int* 2006; **69**: 1786–1791.
4. Ward DT, Yau SK, Mee AP *et al.* Functional, molecular, and biochemical characterization of streptozotocin-induced diabetes. *J Am Soc Nephrol* 2001; **12**: 779–790.
5. Vestergaard P. Discrepancies in bone mineral density and fracture risk in patients with type 1 and type 2 diabetes—a meta-analysis. *Osteoporos Int* 2007; **18**: 427–444.
6. Yamamoto M, Yamaguchi T, Yamauchi M *et al.* Diabetic patients have an increased risk of vertebral fractures independent of BMD or diabetic complications. *J Bone Miner Res* 2009; **24**: 702–709.
7. Guruprakash GH, Krothapalli RK, Rouse D *et al.* The mechanism of hypercalciuria in streptozotocin-induced diabetic rats. *Metabolism* 1988; **37**: 306–311.
8. Ohara N. Impaired intestinal active calcium absorption and reduction of serum 1alpha, 25(OH)2D3 in streptozotocin-induced diabetic pregnant rats with hypocalcemia in their fetuses. *Clin Exp Obstet Gynecol* 2000; **27**: 100–102.
9. Schedl HP, Christensen KK, Ronnenberg WC. Effects of diabetes on calcium uptake by rat brush border membrane vesicles. *Clin Exp Pharmacol Physiol* 1995; **22**: 272–276.
10. Friedman PA, Gesek FA. Cellular calcium transport in renal epithelia: measurement, mechanisms, and regulation. *Physiol Rev* 1995; **75**: 429–471.
11. Garland HO, Harris PJ, Morgan TO. Calcium transport in the proximal convoluted tubule and loop of Henle of rats made diabetic with streptozotocin. *J Endocrinol* 1991; **131**: 373–380.
12. Boland PS, Garland HO. Renal micropuncture study of the effects of D-glucose tubular calcium handling in the anaesthetized rat. *Exp Physiol* 1993; **78**: 175–181.
13. Kuro-o M, Matsumura Y, Aizawa H *et al.* Mutation of the mouse klotho gene leads to a syndrome resembling ageing. *Nature* 1997; **390**: 45–51.
14. Imura A, Tsuji Y, Murata M *et al.* alpha-Klotho as a regulator of calcium homeostasis. *Science* 2007; **316**: 1615–1618.
15. Takeshita K, Fujimori T, Kurotaki Y *et al.* Sinoatrial node dysfunction and early unexpected death of mice with a defect of klotho gene expression. *Circulation* 2004; **109**: 1776–1782.
16. Tsujikawa H, Kurotaki Y, Fujimori T *et al.* Klotho, a gene related to a syndrome resembling human premature aging, functions in a negative regulatory circuit of vitamin D endocrine system. *Mol Endocrinol* 2003; **17**: 2393–2403.
17. Urakawa I, Yamazaki Y, Shimada T *et al.* Klotho converts canonical FGF receptor into a specific receptor for FGF23. *Nature* 2006; **444**: 770–774.
18. Chang Q, Hoefs S, van der Kemp AW *et al.* The beta-glucuronidase klotho hydrolyzes and activates the TRPV5 channel. *Science* 2005; **310**: 490–493.
19. Alexander RT, Woudenberg-Vrenken TE, Buurman J *et al.* Klotho prevents renal calcium loss. *J Am Soc Nephrol* 2009; **20**: 2371–2379.
20. Mogensen CE. Glomerular filtration rate and renal plasma flow in short-term and long-term juvenile diabetes mellitus. *Scand J Clin Lab Invest* 1971; **28**: 91–100.
21. Mogensen CE, Christensen CK, Pedersen MM *et al.* Renal and glycemic determinants of glomerular hyperfiltration in normoalbuminuric diabetics. *J Diabet Complications* 1990; **4**: 159–165.
22. Bohle A, Mackensen-Haen S, Wehrmann M. Significance of postglomerular capillaries in the pathogenesis of chronic renal failure. *Kidney Blood Press Res* 1996; **19**: 191–195.
23. Bohle A, von Gise H, Mackensen-Haen S *et al.* The obliteration of the postglomerular capillaries and its influence upon the function of both glomeruli and tubuli. Functional interpretation of morphologic findings. *Klin Wochenschr* 1981; **59**: 1043–1051.
24. Cha SK, Ortega B, Kurosu H *et al.* Removal of sialic acid involving Klotho causes cell-surface retention of TRPV5 channel via binding to galectin-1. *Proc Natl Acad Sci USA* 2008; **105**: 9805–9810.
25. Imai E, Horio M, Nitta K *et al.* Modification of the Modification of Diet in Renal Disease (MDRD) Study equation for Japan. *Am J Kidney Dis* 2007; **50**: 927–937.
26. Usui HK, Shikata K, Sasaki M *et al.* Macrophage scavenger receptor-a-deficient mice are resistant against diabetic nephropathy through amelioration of microinflammation. *Diabetes* 2007; **56**: 363–372.
27. Kato Y, Arakawa E, Kinoshita S *et al.* Establishment of the anti-Klotho monoclonal antibodies and detection of Klotho protein in kidneys. *Biochem Biophys Res Commun* 2000; **267**: 597–602.
28. van de Graaf SF, Hoenderop JG, Gkika D *et al.* Functional expression of the epithelial Ca(2+) channels (TRPV5 and TRPV6) requires association of the S100A10-annexin 2 complex. *EMBO J* 2003; **22**: 1478–1487.
29. Lu P, Boros S, Chang Q *et al.* The beta-glucuronidase klotho exclusively activates the epithelial Ca2+ channels TRPV5 and TRPV6. *Nephrol Dial Transplant* 2008; **23**: 3397–3402.
30. Yoshimoto S, Nakatani K, Iwano M *et al.* Elevated levels of fractalkine expression and accumulation of CD16+ monocytes in glomeruli of active lupus nephritis. *Am J Kidney Dis* 2007; **50**: 47–58.
31. Nakatani K, Fujii H, Hasegawa H *et al.* Endothelial adhesion molecules in glomerular lesions: association with their severity and diversity in lupus models. *Kidney Int* 2004; **65**: 1290–1300.

Relevant use of Klotho in FGF19 subfamily signaling system in vivo

Ken-ichi Tomiyama[a,b,1], Ryota Maeda[a,b,1], Itaru Urakawa[c], Yuji Yamazaki[c], Tomohiro Tanaka[a,b], Shinji Ito[a,b], Yoko Nabeshima[a,b], Tsutomu Tomita[d], Shinji Odori[d], Kiminori Hosoda[d], Kazuwa Nakao[d], Akihiro Imura[a,b], and Yo-ichi Nabeshima[a,b,2]

[a]Department of Pathology and Tumor Biology, Graduate School of Medicine, Kyoto University, Sakyo-Ku, Kyoto 606-8501, Japan; [c]Pharmaceutical Research Laboratories, Kyowa Hakko Kirin Company, Ltd., Takasaki, Gunma 370-1295, Japan; [b]Core Research for Evolutional Science and Technology, Japan Science and Technology Corporation, Kawaguchi-shi, Saitama 332-0012, Japan; and [d]Department of Medicine and Clinical Science, Graduate School of Medicine, Kyoto University, Sakyo-Ku, Kyoto 606-8501, Japan

Communicated by Yoshito Kaziro, Kyoto University, School of Medicine, Kyoto, Japan, December 9, 2009 (received for review September 28, 2009)

α-Klotho (α-Kl) and its homolog, β-Klotho (β-Kl) are key regulators of mineral homeostasis and bile acid/cholesterol metabolism, respectively. FGF15/ humanFGF19, FGF21, and FGF23, members of the FGF19 subfamily, are believed to act as circulating metabolic regulators. Analyses of functional interactions between α- and β-Kl and FGF19 factors in wild-type, *α-kl*$^{-/-}$, and *β-kl*$^{-/-}$ mice revealed a comprehensive regulatory scheme of mineral homeostasis involving the mutually regulated positive/negative feedback actions of α-Kl, FGF23, and 1,25(OH)$_2$D and an analogous regulatory network composed of β-Kl, FGF15/humanFGF19, and bile acids that regulate bile acid/cholesterol metabolism. Contrary to in vitro data, β-Kl is not essential for FGF21 signaling in adipose tissues in vivo, because (*i*) FGF21 signals are transduced in the absence of β-Kl, (*ii*) FGF21 could not be precipitated by β-Kl, and (*iii*) essential phenotypes in *Fgf21*$^{-/-}$ mice (decreased expressions of *Hsl* and *Atgl* in WAT) were not replicated in *β-kl*$^{-/-}$ mice. These findings suggest the existence of Klotho-independent FGF21 signaling pathway(s) where undefined cofactors are involved. One-to-one functional interactions such as α-Klotho/FGF23, β-Klotho/FGF15 (humanFGF19), and undefined cofactor/FGF21 would result in tissue-specific signal transduction of the FGF19 subfamily.

bile acid | cholesterol | mineral homeostasis | Cyp genes | energy source

The physiological roles of the Klotho family have remained puzzling since the original mutant mouse was developed (1). α-Kl deficiency in mice led to a characteristic phenotype resembling premature aging symptoms in human (1). Thereafter, we found that the overproduction of 1,25(OH)$_2$D and altered mineral-ion homeostasis are the major cause of these premature aging-like phenotypes observed in *α-kl*$^{-/-}$ mice, because the lowering of 1,25(OH)$_2$D activity by dietary restriction (a regimen in which *α-kl*$^{-/-}$ mice are fed a vitamin D–deficient diet) (2) is able to rescue the premature aging–like phenotypes and enable *α-kl*–deficient mice to survive normally without obvious abnormalities. Recently we have reported that α-Kl interacts with fibroblast growth factor 23 (FGF23) in kidney and plays an essential role in maintaining serum 1,25(OH)$_2$D levels by regulation of key active vitamin D–metabolizing enzymes, 1α-hydroxylase (Cyp27b1), and 24-hydroxylalse (Cyp24) (3). We also found that α-Kl binds to Na^+,K^+-ATPase in choroid plexus, parathyroid glands, and the distal convoluted tubules (DCT) of the kidney where extracellular calcium concentration is coordinately regulated (4). In these tissues, Na^+,K^+-ATPase activity is controlled in an α-Kl–dependent manner for transepithelial calcium transport in the choroid plexus and DCT, and for regulated PTH secretion in the parathyroid glands. By associating with both Na^+,K^+-ATPase and circulating FGF23, α-Kl plays a multifunctional role in α-Kl expressing tissues to regulate calcium and phosphate concentrations in vivo. This led to the concept that α-Kl is a regulator that integrates mineral homeostasis (5).

We next identified *β-kl*, which shares structural identity and characteristics with *α-kl* (6). β-Kl is predominantly expressed in the liver, pancreas, and adipose tissues (6) distinct from α-Kl expressing tissues (1, 2). To understand the biological role(s) of β-Kl, we generated a mouse line lacking *β-kl* (7). Although there were no gross abnormalities in the appearance of *β-kl*$^{-/-}$ mice, these mice exhibited an altered metabolism of bile acids, a group of structurally diverse molecules that are primarily synthesized in the liver from cholesterol, promote absorption of dietary lipids in the intestine, and stimulate biliary excretion of cholesterol (8). The enterohepatic circulation of bile acids is regulated largely in hepatocytes where bile acid biosynthesis is regulated by rate-limiting enzymes; cholesterol 7α-hydroxylase (Cyp7a1) and sterol 12α-hydroxylase (Cyp8b1) (8). Bile acids and oxysterols act as ligands to nuclear receptors regulating the expression of important genes in cholesterol homeostasis (9). Particularly, bile acids bind to the promoter region of the farnesoid X receptor (FXR), which induces transcription of small heterodimer partner (SHP), a negative regulator of Cyp7a1 and Cyp8b1, resulting in suppression of bile acids synthesis in a negative feedback manner (9).

Simultaneously, Inagaki et al. reported that FGF15 dramatically suppresses expression of Cyp7a1 through a gut–liver signaling pathway that is different from the FXR/SHP-mediated negative feedback system (10). Moreover, the association of bile acids with FXR leads to the increase of *Fgf15* expression in intestine, resulting in repression of Cyp7a1 in the liver. Importantly, this negative feedback effect was not observed in *Fgf15*$^{-/-}$ and *Fgfr4*$^{-/-}$ mice, and highlighted a concept that the binding of FGF15 with FGFR4 is involved in a second negative feedback system in bile acid metabolism. Taken together, analogous to the role of α-Kl in FGF23/FGFR1-mediated signal transduction, it was hypothesized that β-Kl plays a critical role in FGF15/FGFR4 mediated negative feedback regulation of *Cyp7a1* and *Cyp8b1* expression in the liver (11).

The mammalian FGF family currently consists of 22 members subdivided into seven subfamilies based on their structural similarity and modes of action (12). Most FGFs play an important role as paracrine factors regulating cell growth, regeneration, differentiation, and morphogenesis (13). However, it has been established that members of the FGF-19 subfamily, which also includes FGF21 and FGF23, differ in two important aspects from other FGF proteins. First, they have no or very small mitotic

Author contributions: Y.-i.N. designed research; K.-i.T., R.M., I.U., Y.Y., T. Tanaka, S.I., Y.N., and S.O. performed research; T. Tomita, K.H., K.N., and A.I. analyzed data; and A.I. and Y.-i.N. wrote the paper.

The authors declare no conflict of interest.

Freely available online through the PNAS open access option.

[1]K.-i.T. and R.M. contributed equally to this work.

[2]To whom correspondence should be addressed. E-mail: nabemr@lmls.med.kyoto-u.ac.jp.

This article contains supporting information online at www.pnas.org/cgi/content/full/0913986107/DCSupplemental.

effects; and second, they exert their action via systemic, hormone-like effects as metabolic regulators. In fact, human FGF19 (hFGF19) and its murine ortholog FGF15, as well as FGF23, are secreted from ileal enterocytes and bone, respectively, and then circulate in the bloodstream to target tissues (12–14). The third member, FGF21 is predominantly synthesized in the liver (15) and has beneficial effects on several metabolic parameters in different animal models of obesity; recently, FGF21 has been postulated to be a newly found regulator of glucose metabolism through induction of glucose transporter 1 (GLUT 1) (16).

As first shown for FGF23 and subsequently for FGF19, FGF21 has been predicted to require a specific cofactor for its binding to a certain type of FGFR and subsequent activation of FGF21/FGFR signaling pathway. β-Kl has been reported as a candidate cofactor essential for bioactivity of FGF21 in in vitro studies (16–22). However, these have not been confirmed in in vivo studies. It is particularly important to examine (*i*) whether FGF21 signal transduction is abolished in *β-kl*$^{-/-}$ mice and (*ii*) whether the phenotypes of *β-kl*$^{-/-}$ mice significantly overlap with those of *Fgf21*-deficient mice (*Fgf21*$^{-/-}$) (23, 24).

Recent advances in understanding the signaling of FGF19 subfamilies have mainly been based on conventional in vitro experiments (13, 17, 19, 22), whereas in vivo verification of the association of FGF ligands and FGF receptor or of FGF ligands and Klotho family proteins, as well as the signal transduction (phosphorylation) cascades triggered by FGF 19 subfamilies have yet to be confirmed.

In the present study, we demonstrate the first manifest evidence revealing that whereas α-Kl and β-Kl are required for FGF23 and FGF15/hFGF19-mediated signaling pathways in vivo, respectively, β-Kl appears not to be essential for FGF21-mediated signal transduction in vivo.

Results

α-Kl–Dependent Vitamin D Regulation by FGF23. FGF23 is derived from bone and is essential for maintaining phosphate homeostasis and regulation of vitamin D metabolism. In WT mice, administration of hFGF23 results in remarkable suppression of serum 1,25-dihydroxyvitamin D [1,25(OH)$_2$D] through the repression of *Cyp27b1* and induction of *Cyp24* in the kidney. As we previously reported, serum concentrations of 1,25(OH)$_2$D in both *α-kl*$^{-/-}$ and *Fgf23*$^{-/-}$ mice were remarkably higher than that of WT mice (2, 25). Intriguingly, serum FGF23 in *α-kl*$^{-/-}$ mice was >8,000-fold that of WT mice (Fig. 1*A*). To analyze how α-Kl and FGF23 coordinately regulate vitamin D metabolism in the kidney, we analyzed the interactive actions of FGF23 and α-Kl in vivo. The FGFs used in these experiments (hFGF23, hFGF19, hFGF21) were prepared from CHO cell culture media, and their activities were estimated by measuring *Egr-1*-promotor directed Luciferase activities using Peak rapid cells with or without exogenous expression of *α-kl* or *β-kl* (Fig. S1). Furthermore the activity of hFGF21 was confirmed by up-regulation of *Glut1* mRNA in 3T3-L1 adipocyte. To minimize the effects of hypervitaminosis D, a major cause of the abnormalities observed in *α-kl*$^{-/-}$ mice, we used *α-kl*$^{-/-}$ mice fed with a vitamin D–deficient diet, in which serum 1,25(OH)$_2$D levels were normal and consequently most of the premature aging–like phenotypes were alleviated (2).

hFGF23 administration induced a significant decrease in serum 1,25(OH)$_2$D levels in WT mice, whereas no effect was observed in *α-kl*$^{-/-}$ mice (Fig. 1*B*). Consistently, in WT kidneys injected with hFGF23, *Cyp27b1* expression was reduced >13-fold, whereas *Cyp24* expression was induced >5-fold (Fig. 1 *C* and *D*). However, no significant effect of hFGF23 was found on the expression of *Cyp27b1* and *Cyp24* in *α-kl*$^{-/-}$ mice. These results offer direct evidence that α-Kl is essential for FGF23-derived repression of *Cyp27b1* and induction of *Cyp24* in vivo. In addition, we found that the administration of hFGF23 resulted in down-regulation of α-Kl expression (Fig. 1*E*), probably because α-Kl is a target of FGF23 signal transduction and/or because of a secondary effect of decreased 1,25(OH)$_2$D, an inducer of α-Kl gene expression (2). These data implicate an elaborate mutual negative feedback system composed of α-Kl, FGF23, and 1,25(OH)$_2$D in mineral-ion maintenance (Fig. 5*A*).

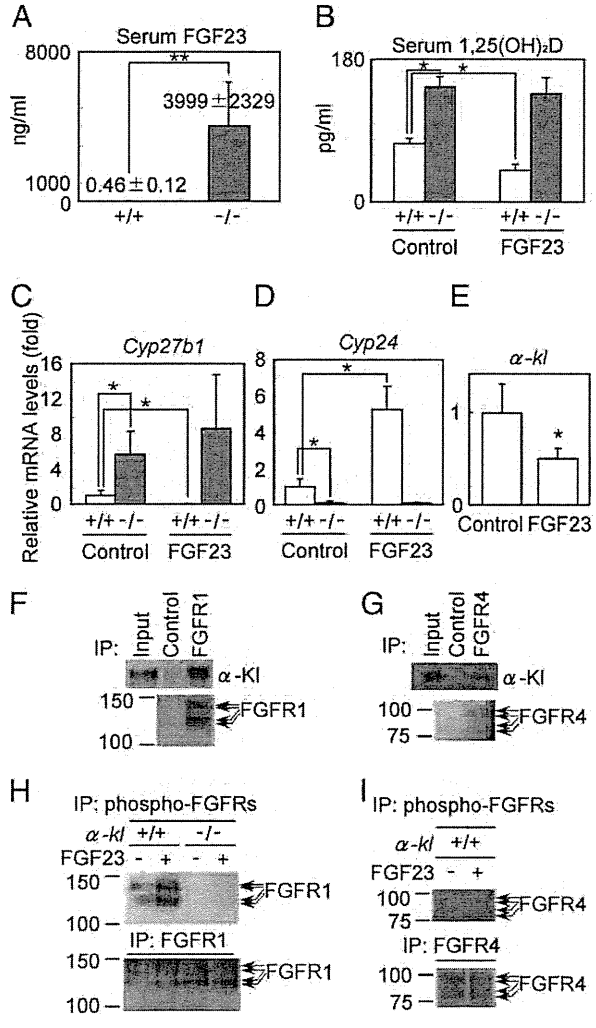

Fig. 1. FGF23 is dependent on α-Kl for regulation of vitamin D synthesis in kidney (*A–E*). (*A*) Serum concentrations of FGF23 in WT and *α-kl*$^{-/-}$ were measured by ELISA. WT (*open bars*) and *α-kl*$^{-/-}$ (*filled bars*) mice (n = 4/group) were injected with recombinant hFGF23 (0.2 mg/kg) or PBS control. Mice were killed 4 h after injection, and serum concentrations of 1,25(OH)$_2$D (*B*) were measured. *Cyp27b1* (*C*), *Cyp24* (*D*), and *α-kl* (*E*) mRNA levels in kidney were analyzed by RT–quantitative PCR. In this and all other figures, error bars represent mean ± SD and are plotted as fold change. Data were derived from 8- to 10-week-old male mice on vitamin D–deficient diets. *$P < 0.05$; **$P < 0.01$. FGFR1 binds to α-Kl and is phosphorylated by FGF23 in the kidney (*F–I*). (*F*) Kidney lysates were precipitated with anti-FGFR1 antibody or with control IgG. Input is 0.01% of the kidney whole extract used for the immunoprecipitation. (*G*) Kidney lysates were precipitated with anti-FGFR4 antibody or with control IgG. Input is 0.2% of the kidney whole extract used for the immunoprecipitation. (*H*) The kidney lysates of WT and *α-kl*$^{-/-}$ mice were immunoprecipitated with the anti-phospho-FGFRs or the anti-FGFR1 antibody. The immunoprecipitates were separated by SDS/PAGE and blotted with anti-FGFR1 antibody. (*I*) Kidney lysates of WT mice were immunoprecipitated with the anti–phospho-FGFRs or the anti-FGFR4 antibody and then blotted with anti-FGFR4 antibody.

α-Kl–Dependent FGFR1 Phosphorylation by FGF23 in Vivo. Generally FGFs can bind to and activate cell surface tyrosine kinase FGF receptors and transduce signals to downstream molecules including MAP kinase (26). The FGF receptor family consists of

four members, FGFR1–4. With the exception of FGFR4, splicing variants in the third Ig-like domain (IIIb and IIIc types) have been identified for each member (12, 26). Recently, it has been reported that α-Kl binds to FGFRs in cultured cells (19) and converts the canonical FGFR1(III)c to a receptor specific for FGF23 (3). We therefore tested whether the above observations were valid in vivo. We first examined the interactions between α-Kl and FGFR1, and α-Kl and FGFR4 in the kidney. As observed in in vitro experiments, α-Kl was coprecipitated not only with FGFR1 but also with FGFR4 in the kidney (Fig. 1*F* and *G*). We then investigated whether these two receptors are activated by hFGF23 in the kidney (procedures are as in *SI Text* and Fig. S2). In WT mice, FGFR1 was activated in the kidney 10 min after injection of hFGF23 (Fig. 1*H*). In contrast, phosphorylation of FGFR4 was not detectable even after the injection of hFGF23 (Fig. 1*I*), suggesting that FGFR4 is not a major receptor responsible for FGF23 signaling in the kidney. As expected, we could not detect phosphorylation of FGFR1 in the kidney of $\alpha\text{-}kl^{-/-}$ mice even after hFGF23 injection (Fig. 1*H*). In summary, we concluded that FGFR1 is preferentially activated by FGF23 in a α-Kl–dependent manner in the kidney.

β-Kl–Dependent Bile Acid Regulation by FGF15. Because the unusually elevated expression of Cyp7a1 was observed not only in $\beta\text{-}kl^{-/-}$ mice (7) but also in $Fgf15^{-/-}$ and $Fgfr4^{-/-}$ mice (10, 27), we predicted that β-Kl was involved in FGF15/FGFR4-signaling system. Based on studies in cultured cells, it was recently proposed that β-Kl is necessary for FGF15/hFGF19-mediated signal transduction in the liver (18, 22). To confirm this hypothesis in vivo, we first measured the mRNA levels of *Fgf15* in the terminal ileum of WT and $\beta\text{-}kl^{-/-}$ mice. Interestingly, *Fgf15* expression levels were ~12-fold increased in $\beta\text{-}kl^{-/-}$ mice compared with those of WT (Fig. 2*A*), analogous to the elevation of FGF23 expression in $\alpha\text{-}kl^{-/-}$ mice (Fig. 1*A*). To evaluate the effect of FGF15 in vivo, we administered hFGF19 and analyzed *Cyp7a1* and *Cyp8b1* expression. In WT mice, the expression levels of *Cyp7a1* and *Cyp8b1* 6 h after hFGF19 injection resulted in >100-fold and >10-fold reductions, respectively (Fig. 2 *B* and *C*). These were comparable to findings in a previous study examining FGF15 (10), and thus we concluded hFGF19 could be used to evaluate bile acid regulation in mice. In contrast, the expression levels of *Cyp7a1* and *Cyp8b1* remained elevated in $\beta\text{-}kl^{-/-}$ livers even after the administration of hFGF19 (Fig. 2 *B* and *C*), demonstrating that β-Kl is essential for the negative regulation of Cyp7a1 and Cyp8b1 by FGF15/hFGF19 in vivo. β-Kl-regulated bile acid synthesis by FGF15/hFGF19 is further described in *SI* (Fig. S3).

β-Kl/FGFR4 Coexpression Is Required for FGF15 Signaling in Vivo. To monitor whether FGF15/hFGF19 signals are transduced in tissues other than the liver, we verified *Egr-1* (a zinc-finger transcription factor identified as an immediate-early gene induced by cellular stimulation) mRNA levels in β-Kl–expressing tissues (liver, adipose, pancreas, and salivary gland) as well as several β-Kl–nonexpressing tissues, since hFGF23 administration remarkably increased *Egr-1* expression and induced phosphorylation of 44/42 MAP kinase (ERK1/2) in the kidney where α-Kl is expressed (3). In WT liver, *Egr-1* expression level increased by >120-fold 30 min after hFGF19 administration compared with vehicle (Fig. 2*D*). With respect to other tissues, we observed a faint, but statistically significant *Egr-1* increase in pancreas (>5-fold) and in white adipose tissue (WAT) (~3-fold). Nonetheless, no remarkable changes were observed in other tissues including brown adipose tissue (BAT) and salivary gland despite β-Kl expression. As expected, in $\beta\text{-}kl^{-/-}$ mice injected with hFGF19, no significant induction of *Egr-1* was observed in any of the tissues evaluated (Fig. 2*D*), demonstrating that β-Kl is necessary but not sufficient for FGF15/hFGF19-mediated signal transduction. To address the question of why FGF15/hFGF19 signal is transduced in the liver, pancreas, and WAT, but not in BAT and

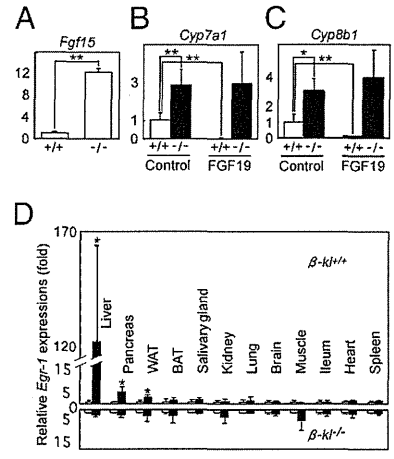

Fig. 2. FGF19 is dependent on β-Kl for regulation of bile acid synthesis in liver (*A–D*). (*A*) mRNA levels of *Fgf15* in terminal ileum in WT and $\beta\text{-}kl^{-/-}$ were measured by RTQ-PCR. WT mice (*open bars*) and $\beta\text{-}kl^{-/-}$ mice (*filled bars*) ($n = 5$/group) were injected with recombinant hFGF19 (1 mg/kg) or control medium. Mice were killed 6 h after injection and *Cyp7a1* (*B*) and *Cyp8b1* (*C*) mRNA levels in liver were measured by RT–quantitative PCR. Data were derived from 14- to 16-week-old male mice on standard diet. Egr-1 induction mediated by FGF19 in liver (*D*). hFGF19 (1 mg/kg) or control medium were injected into WT and $\beta\text{-}kl^{-/-}$ male mice (12–14 weeks old) on standard diet. Thirty minutes after injection, tissues in WT (*Upper*) and $\beta\text{-}kl^{-/-}$ (*Lower*) mice ($n = 4$/group) were excised. *Egr-1* mRNA levels were measured by RT-quantitative PCR. The expression levels of FGF19-injected mice (*filled bars*) and vehicle injected mice (*open bars*) are plotted as fold change. $*P < 0.05$; $**P < 0.01$.

salivary glands, we profiled the expression of various FGF receptors (FGFRs) in β-Kl–expressing tissues. As reported previously (10), FGFR4 is postulated to be the major receptor responsible for FGF15-mediated signal transduction in the liver. As for the pancreas and WAT, we did observe >2-fold and >6-fold lower *Fgfr4* expression compared with that in the liver, respectively. On the contrary, *Fgfr4* mRNA was not detected in the salivary glands and BAT (Fig. S4). Hence *Egr-1* up-regulation by hFGF19 could be observed in tissues where β-Kl and FGFR4 are coexpressed.

To further demonstrate the contribution of β-Kl in the hepatic FGF15/hFGF19-mediated signaling cascade, we evaluated the phosphorylation of FGFR4 and downstream signaling molecules in vivo using the methods shown in Fig. 1 (Fig. S2 and *SI Text*). β-Kl could be efficiently precipitated by an anti-FGFR4 antibody (Fig. 3*A*) and the phosphorylation of FGFR4 was confirmed after hFGF19 treatment in WT liver (Fig. 3*B*). Unexpectedly, the amount of FGFR4 protein was significantly reduced in livers of $\beta\text{-}kl^{-/-}$ mice (Fig. 3*C*). To obtain an amount of FGFR4 equivalent to that obtained from WT mice, we concentrated the liver lysates from $\beta\text{-}kl^{-/-}$ mice and performed immunoprecipitation (Fig. S2 and *SI Text*). However, we could not detect enhanced activation of FGFR4 in $\beta\text{-}kl^{-/-}$ livers even after injection of hFGF19 (Fig. 3*D*). Consistent with a previous report (18), clear phosphorylation of ERK1/2 was observed in WT livers 10 min after hFGF19 injection, whereas it was undetectable in $\beta\text{-}kl^{-/-}$ livers (Fig. 3*E*), demonstrating that β-Kl is essential for the FGF15/hFGF19 directed activation of FGFR4 and downstream signaling cascade in the liver.

β-Kl Is Not Essential for FGF21-Mediated Signaling in Adipose Tissues. FGF21, a member of the FGF19 subfamily that is synthesized in the liver, has been reported to be a newly found regulator of glucose metabolism (16) and β-Kl has been postulated to be essential for its activity in in vitro studies (17, 20, 21). To examine the possible contribution of β-Kl in the FGF21 signaling system in vivo, we first administered recombinant hFGF21 to WT mice and analyzed *Egr-1* mRNA levels in multiple tissues (Fig. 4*A*). Before its use, we con-

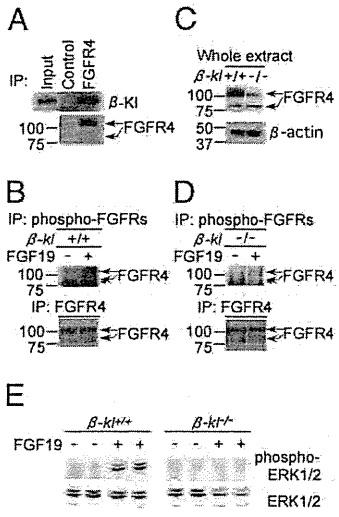

Fig. 3. FGFR4 binds to β-Kl and is phosphorylated by FGF19 in liver. (*A*) Liver lysates were precipitated with anti-FGFR4 antibody or with control IgG. Input is 1% of the liver whole extract used for the immunoprecipitation. The immunoprecipitates were separated by SDS/PAGE and blotted with anti-FGFR4 antibody. (*B, D,* and *E*) Ten minutes after injection of hFGF19 or control medium, livers were excised. Liver lysates from WT mice (*B*) and β-$kl^{-/-}$ mice (*D*) were immunoprecipitated with the anti–phospho-FGFRs or the polyclonal anti-FGFR4 antibody. Immunoprecipitates were blotted with anti-FGFR4 antibody. The arrowhead indicates a nonspecific band (Fig. S2). (*C*) Whole liver extracts of WT and β-$kl^{-/-}$ mice were blotted with anti-FGFR4 antibody or anti–β-actin antibody for a loading control. (*E*) Liver lysates from WT and β-$kl^{-/-}$ were immunoblotted with anti-phospho-ERK1/2 or anti-ERK1/2 antibodies ($n = 2$ in each case).

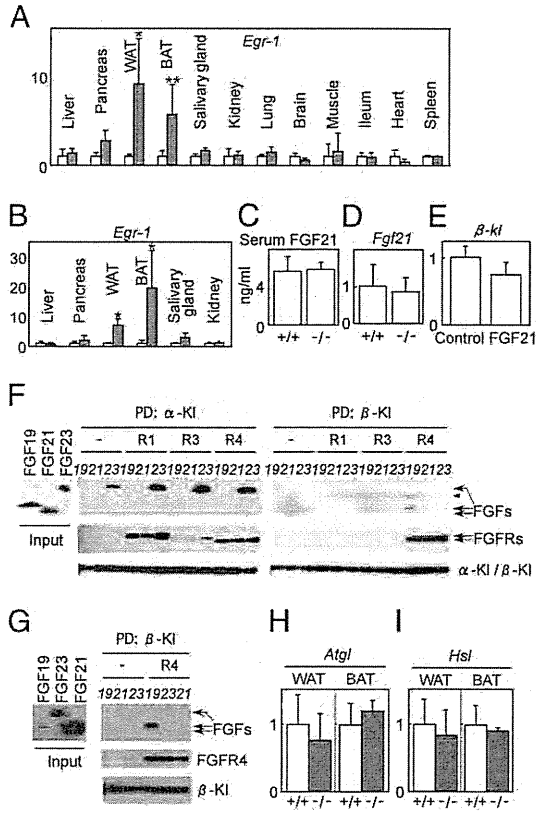

Fig. 4. β-Kl is not essential for FGF21-mediated signaling (*A–I*). Thirty minutes after injection, tissues in WT ($n = 5$/group) (*A*) and β-$kl^{-/-}$ mice ($n = 4$/group) (*B*) were excised. *Egr-1* mRNA levels were measured by RT-quantitative PCR. The expression levels of hFGF21 injected mice (*filled bars*) and vehicle injected mice (*open bars*) mice are plotted as fold change. Data were derived from 7- to 10-week-old male mice on standard diet. (*C*) Serum FGF21 concentrations of WT and β-$kl^{-/-}$ mice ($n = 5$–6/group) were measured by RIA. (*D*) *Fgf21* mRNA levels in livers of WT and β-$kl^{-/-}$ mice ($n = 5$–6/group) were measured by RT-quantitative PCR and are plotted as fold change. Data were derived from 15- to 20-week-old male mice on standard diet. hFGF21 (0.4 mg/kg) or control medium were injected into WT and β-$kl^{-/-}$ mice. (*E*) WT mice were injected with recombinant hFGF21 (0.4 mg/kg) or control medium ($n = 5$/group). Mice were killed 4 h after injection and β-*kl* mRNA levels in WAT were analyzed by RT-quantitative PCR. Data were derived from 10-week-old male mice on standard diet. (*F*) A 15-ng quantity of each FGF was pulled down (PD) by α-/β-Kl in the presence (R1, R3, or R4) or absence (–) of FGFRs. Input was 8% of samples used for the pull-down assay. Samples of pulled down by α-/β-Kl were analyzed by SDS/PAGE and blotted with antibodies (anti-His for FGFs, anti-Human Fc for FGFRs, and anti-GFP for α-/β-Kl). Arrowhead indicates a nonspecific band. (*G*) A 50-ng quantity of FGF19, 150 ng of FGF23, or 500 ng of FGF21 was precipitated by β-Kl in the presence or absence of FGFR4. Input was 1% of samples used for the assay. (*H* and *I*) *hsl* and *atgl* mRNA levels in WAT and BAT were analyzed by RT-quantitative PCR. Data were derived from 9- to 14-week-old female β-$kl^{+/+}$ and β-$kl^{-/-}$ mice ($n = 5$/group). $^*P < 0.05$; $^{**}P < 0.01$.

firmed the biological activity of the synthesized hFGF21. As shown in Fig. S5, our hFGF21 could enhance *Egr1*-derived luciferase reporter expression in a β-Kl–dependent manner at doses that were equivalent to those previously reported (17, 21). Moreover the hFGF21 up-regulated *Glut1* mRNA in 3T3-L1 adipocyte (Fig. S5) (16). Consistent with the in vitro results, in WT mice, *Egr-1* expression levels were significantly up-regulated by ~10-fold in WAT and >6-fold in BAT 30 min after injection of hFGF21 (Fig. 4*A* and Fig. S5). However, administration of hFGF21 also resulted in significant up-regulation of *Egr-1* mRNA levels in WAT and BAT from β-$kl^{-/-}$ mice (Fig. 4*B*). We next analyzed the serum levels of FGF21 and hepatic mRNA levels of *Fgf21* in WT and β-$kl^{-/-}$ mice. Unexpectedly, there was no significant genotype-dependent difference in mean serum protein concentrations of FGF21 nor hepatic *Fgf21* mRNA levels (Fig. 4 *C* and *D*). We also confirmed that β-*kl* expression was not affected by FGF21 administration (Fig. 4*E*). These results suggest that β-Kl is not essential for FGF21-mediated signaling in WAT and BAT. In addition, our prediction was further supported by the following experiments. First, to address the binding properties between β-Kl and FGF21, we performed pull-down assays using recombinant proteins. Although FGF19 was significantly bound by β-Kl in the presence of FGFR4, FGF21 could not be precipitated by β-Kl even with 10 fold amounts of FGF21 (Fig. 4 *F* and *G* and *SI Text*). Second, we compared the phenotypes of $Fgf21^{-/-}$ and β-$kl^{-/-}$ mice. Recently, Hotta et al. developed $Fgf21^{-/-}$ mice and reported that expression levels of hormone-sensitive lipase (*Hsl*) and adipose triglyceride lipase (*Atgl*) in WAT were decreased in $Fgf21^{-/-}$ mice to almost 50% compared with those of WT mice (23). The adipose phenotypes in $Fgf21^{-/-}$ mice may be an outcome of a deficiency in FGF21 signaling. Thus we analyzed the expression levels of these genes in the adipose tissues of β-$kl^{-/-}$ mice. Consequently, in both WAT and BAT, mRNA levels of *Hsl* and *Atgl* were not significantly altered between WT and β-$kl^{-/-}$ mice (Fig. 4 *H* and *I*). These data suggest that β-Kl may not necessarily be involved in the phenotypes observed in FGF21-deficient mice. Taken together, these results provide strong evidence that β-Kl is not essential for FGF21-mediated signaling in WAT and BAT. We therefore asked whether FGF21 signaling might require other unidentified components than β-Kl. We also analyzed *Glut1* mRNA levels 4 h after hFGF21 injection at concentrations that could induce *Egr-1* expression in WAT and BAT, but no apparent induction was observed, suggesting that *Glut1* is not a direct target of FGF21 signaling (28, 29).

Discussion

Various roles of Klotho family members have been reported (18, 22, 30); however, a consensus on the molecular functions of α-Kl

and β-Kl has not been reached. Based on these findings, we propose a comprehensive regulatory scheme of mineral homeostasis that is illustrated by the mutually regulated positive/negative feedback actions of α-Kl, FGF23, and $1,25(OH)_2D$ (Fig. 5*A*). In the present study, we found that FGF23 represses the expression of α-Kl and identified an essential role of α-Kl in FGF23-mediated phosphorylation of FGFR1 in the kidney. This leads to *Cyp27b1* down-regulation and *Cyp24* up-regulation, and results in inhibition of the synthesis of $1,25(OH)_2D$, an active form of vitamin D (3). $1,25(OH)_2D$ has prominent effects on the kidney, intestine, and bone. In the kidney, $1,25(OH)_2D$ activates vitamin D receptor (VDR) by binding to its ligand binding domain and negatively regulates the expression of *Cyp27b1* while positively regulating *Cyp24* and α-Kl expression (2). In the bone, $1,25(OH)_2D$ binds to VDR and induces FGF23 synthesis in osteocytes and osteoblasts (31) in hours/days. In turn, secreted FGF23 suppresses $1,25(OH)_2D$ synthesis and inorganic phosphate reabsorption in the kidney to adjust extracellular mineral concentrations. Collectively, α-Kl, in combination with FGF23, is involved in a signaling cascade that maintains extracellular calcium/phosphate levels within a narrow range.

The roles of β-Kl, FGF15, and FGFR4 in bile acid/cholesterol metabolism are schematically summarized in Fig. 5*B*. Consistent with a previous study (10, 22), i.v. injection of hFGF19 dramatically represses the expression of *Cyp7a1* and *Cyp8b1* and results in the inhibition of bile acid synthesis from cholesterol in WT livers. This suppression of *Cyp7a1* and *Cyp8b1* was not observed in *β-kl*$^{-/-}$ mice. Indeed, phosphorylation of FGFR4 and ERK1/2 was not detected in *β-kl*$^{-/-}$ livers even after hFGF19 administration. Our findings provide conclusive evidence proving the essential role of β-Kl in FGF15/hFGF19-mediated activation of FGFR4 and subsequent signal transduction that regulates bile acid synthesis. Particularly, by binding to FXR, bile acid induces SHP expression in the liver and FGF15 transcription in the terminal ileum. In turn, increased SHP and secreted FGF15 differentially suppress Cyp7a1/Cyp8b1 expression to down-regulate bile acid synthesis (8, 9, 11). In addition, we found mutual negative feedback regulations between β-Kl and FGF15, namely, a decrease in *β-kl* after hFGF19 administration and an increase in *Fgf15* in *β-kl* deficiency. In other words, *β-kl* ablation leads to impaired negative feedback regulation of bile acid metabolism, resulting in the overflow of bile acid pools. Consequently, in the *β-kl*$^{-/-}$ terminal ileum, chronic stimulation by elevated bile acid would lead to an unusual increase in *Fgf15* mRNA. We propose a scheme illustrating the bile acid/cholesterol homeostasis regulated by mutual negative/positive feedback actions of β-Kl, FGF15, and bile acids (Fig. 5*B*).

As shown in Fig. 5, the scheme for bile acid regulation by β-Kl/FGF15 is conceptually analogous to that of vitamin D metabolism, which involves α-Kl and FGF23. Both systems are regulated by the coordination of two types of feedback mechanisms mediated by end-metabolites, $1,25(OH)_2D$ or bile acids, that are in situ negative feedback regulation and target tissue mediated negative feedback loop. In the former pathway, the end-metabolite functions as a nuclear receptor ligand and negatively feeds back by repressing the expression of key regulatory enzymes (Cyp27b1 in the kidney or Cyp7a1/Cyp8b1 in the liver) in the relevant metabolic pathway responsible for the generation of end-metabolite itself. In the latter system, the end-metabolite is transported to the target tissue (bone or intestine) from a distal site and enhances the expression of FGF (FGF23 or FGF15) by binding to the nuclear receptor; VDR or FXR. Subsequently, secreted FGF acts as the regulator of a target tissue–mediated negative feedback loop in collaboration with α-Kl or β-Kl. The next question to be addressed is how these two pathways are coordinately involved in the rapid adjustment and long term maintenance of mineral homeostasis and bile acid metabolism.

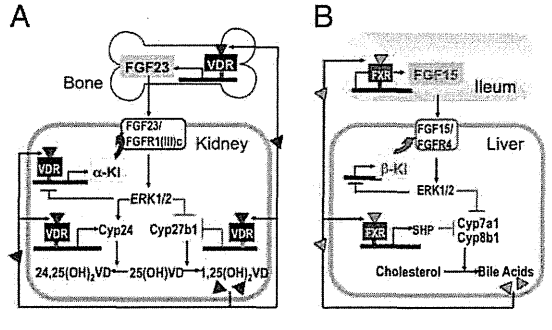

Fig. 5. Schematic representation of α-Kl/FGF23 and β-Kl/FGF15 systems. (*A*) Regulatory network of mineral homeostasis illustrated by the mutual positive/negative feedback actions of α-Kl, FGF23, and $1,25(OH)_2D$. (*B*) Regulatory network of bile acid/cholesterol metabolism represented by the mutual positive/negative feedback actions of β-Kl, FGF15, and bile acids.

In a previous report, we showed that i.v. injection of hFGF23 induces phosphorylation of ERK1/2 and specifically up-regulates the expression of *Egr-1* in the murine kidney (3). Here we demonstrate that α-Kl is required for FGF23 signal transduction in vivo. Likewise, i.v. injection of hFGF19 results in ERK1/2 phosphorylation and up-regulation of *Egr-1* in the liver in a β-Kl–dependent manner. Among β-Kl–expressing organs, significant up-regulation of *Egr-1* was observed in tissues where β-Kl and FGFR4 are coexpressed. Although induction of *Egr-1* in pancreas and WAT are slight, it occurs in a β-Kl–dependent manner. FGF15-mediated signal in pancreas and WAT could therefore be involved in bile acid homeostasis, but its functional importance has yet to be elucidated. Furthermore, the very high *Egr-1* induction in the liver strongly suggests that other elements, in addition to the coexpression of β-Kl and FGFR4, may endow this prominent hepatic signal activation. Recently, several groups have reported that α-Kl and β-Kl can bind to certain types of FGFRs. Those studies report preferences and differences for this binding that might be dependent on assay conditions. α-Kl solely binds to FGFR1(IIIc) in vitro (3), however α-Kl binds to not only FGFR1(IIIc) but also FGFR4 and weakly to FGFR3(IIIc) in cultured cells (30). Even though FGFR4 could precipitate α-Kl in the kidney, activation of FGFR4 by hFGF23 could not be detected. Further studies are required to understand how FGFR(s) is definitively and preferentially used for a particular FGF signal in vivo.

Serum levels of FGF23 and ileac *Fgf15* mRNA expression were intensively increased in *α-kl*$^{-/-}$ and *β-kl*$^{-/-}$ mice, respectively. Furthermore, administrations of hFGF23 and hFGF19 apparently suppressed the expression of *α-kl* and *β-kl*, respectively. In contrast, the serum levels of FGF21 and hepatic *Fgf21* mRNA expression were not increased in *β-kl*$^{-/-}$ mice, and *β-kl* expression was not significantly suppressed by hFGF21 in adipose. Consistent with a previous report that FGF21 induces ERK1/2 phosphorylation specifically in WAT (17), administration of FGF21 to WT mice significantly induced *Egr-1* mRNA expression in WAT and BAT, suggesting that WAT and BAT were the possible target tissues of FGF21. However, surprisingly, remarkable *Egr-1* inductions in WAT and BAT were also observed in *β-kl*$^{-/-}$ mice, indicating that β-Kl is not essential for FGF21 signal transduction in vivo. These in vivo results contrasted with those obtained from in vitro assays, as β-Kl is essential for FGF21-mediated signal transduction in vitro. We reproduced the direct binding of α-Kl and hFGF23 and also confirmed tricomplex formation of β-Kl, hFGF19, and FGFR4 but were unable to detect binding of α-/β-Kl and hFGF21 in our pull-down assay (Fig. 4*G*). Furthermore, we confirmed that the adipose phenotypes in *Fgf21*$^{-/-}$ mice did not overlap with those of *β-kl*$^{-/-}$ mice. This inconsistency leads to a postulation that β-Kl is not necessary for FGF21 signaling.

Currently, β-Kl is believed to be a common player essential for FGF15- and FGF21-mediated signal transduction. However, our present results, together with the data from Hotta et al. (23), do

not support this hypothesis. Possible explanations are that the response found in cultured cells might be caused by: (*i*) an artificial abundance of β-Kl and/or FGF21, (*ii*) peculiar characteristics of the cultured cells used in these experiments, and/or (*iii*) a combination of these two factors (17, 20, 21).

Recent studies have reported that FGF21 stimulates lipolysis in WAT and ketogenesis in the liver (32, 33). However, those results represent the pharmacological effects of sustained FGF21 treatment and thus include consequences that are secondary and indirectly induced by FGF21. We propose a β-Kl–independent response directly triggered by hFGF21 administration. Significant *Egr-1* upregulation in WAT and BAT are indicative that FGF21 mediates lipid metabolism in adipose tissues. The physiological target(s) of FGF21 signaling need to be clarified to understand how FGF21 functions as a regulator of lipid metabolism. Observations using genetic manipulation will lead us to a precise understanding of the roles of the FGF19 subfamily in metabolic homeostasis in vivo.

Materials and Methods

Measurement of Serum Parameters. Blood samples were collected from orbital cavities or hearts under anesthesia and were centrifuged to obtain sera. Serum FGF23 levels were measured by sandwich ELISA (Kainos Laboratory), which can quantify the intact form or FGF23 using human recombinant FGF23 as a standard. Serum $1,25(OH)_2D$ levels were analyzed by SRL, Inc. Serum FGF21 levels were measured by specific RIA (Phoenix Pharmaceuticals, Inc.).

Statistical Analysis. Unless otherwise noted, all values are expressed as mean ± SD. All data were analyzed by the Mann–Whitney *U* test. *P* values less than 0.05 were considered to be statistically significant.

More details are described in *SI Materials and Methods.*

ACKNOWLEDGMENTS. We thank Drs. M. Murata and R.Yu for critical reading of the manuscript and M. Terao and K. Yurugi for support in our experiments. This work was supported Ministry of Education, Science and Culture Grants 19045016 and 21390058 (to A.I.) and 17109004 (to Y-I.N.) and Ministry of Health and Welfare, and Labor Grant H16-genome-005 (to Y-I.N.).

1. Kuro-o M, et al. (1997) Mutation of the mouse Klotho gene leads to a syndrome resembling ageing. *Nature* 390:45–51.
2. Tsujikawa H, Kurotaki Y, Fujimori T, Fukuda K, Nabeshima Y (2003) Klotho, a gene related to a syndrome resembling human premature aging, functions in a negative regulatory circuit of vitamin D endocrine system. *Mol Endocrinol* 17:2393–2403.
3. Urakawa I, et al. (2006) Klotho converts canonical FGF receptor into a specific receptor for FGF23. *Nature* 444:770–774.
4. Imura A, et al. (2007) alpha-Klotho as a regulator of calcium homeostasis. *Science* 316: 1615–1618.
5. Nabeshima Y, Imura H (2008) alpha-Klotho: A regulator that integrates calcium homeostasis. *Am J Nephrol* 28:455–464.
6. Ito S, et al. (2000) Molecular cloning and expression analyses of mouse betaklotho, which encodes a novel Klotho family protein. *Mech Dev* 98:115–119.
7. Ito S, et al. (2005) Impaired negative feedback suppression of bile acid synthesis in mice lacking betaKlotho. *J Clin Invest* 115:2202–2208.
8. Russell DW (2003) The enzymes, regulation, and genetics of bile acid synthesis. *Annu Rev Biochem* 72:137–174.
9. Goodwin B, et al. (2000) A regulatory cascade of the nuclear receptors FXR, SHP-1, and LRH-1 represses bile acid biosynthesis. *Mol Cell* 6:517–526.
10. Inagaki T, et al. (2005) Fibroblast growth factor 15 functions as an enterohepatic signal to regulate bile acid homeostasis. *Cell Metab* 2:217–225.
11. Jones S (2008) Mini-review: Endocrine actions of fibroblast growth factor 19. *Mol Pharm* 5:42–48.
12. Itoh N, Ornitz DM (2004) Evolution of the Fgf and Fgfr gene families. *Trends Genet* 20:563–569.
13. Itoh N, Ornitz DM (2008) Functional evolutionary history of the mouse Fgf gene family. *Dev Dyn* 237:18–27.
14. Nishimura T, Utsunomiya Y, Hoshikawa M, Ohuchi H, Itoh N (1999) Structure and expression of a novel human FGF, FGF-19, expressed in the fetal brain. *Biochim Biophys Acta* 1444:148–151.
15. Nishimura T, Nakatake Y, Konishi M, Itoh N (2000) Identification of a novel FGF, FGF-21, preferentially expressed in the liver. *Biochim Biophys Acta* 1492:203–206.
16. Kharitonenkov A, et al. (2005) FGF-21 as a novel metabolic regulator. *J Clin Invest* 115: 1627–1635.
17. Ogawa Y, et al. (2007) BetaKlotho is required for metabolic activity of fibroblast growth factor 21. *Proc Natl Acad Sci USA* 104:7432–7437.
18. Kurosu H, et al. (2007) Tissue-specific expression of betaKlotho and fibroblast growth factor (FGF) receptor isoforms determines metabolic activity of FGF19 and FGF21. *J Biol Chem* 282:26687–26695.
19. Wu X, et al. (2007) Co-receptor requirements for fibroblast growth factor-19 signaling. *J Biol Chem* 282:29069–29072.
20. Suzuki M, et al. (2008) betaKlotho is required for fibroblast growth factor (FGF) 21 signaling through FGF receptor (FGFR) 1c and FGFR3c. *Mol Endocrinol* 22:1006–1014.
21. Kharitonenkov A, et al. (2008) FGF-21/FGF-21 receptor interaction and activation is determined by betaKlotho. *J Cell Physiol* 215:1–7.
22. Lin BC, Wang M, Blackmore C, Desnoyers LR (2007) Liver-specific activities of FGF19 require Klotho beta. *J Biol Chem* 282:27277–27284.
23. Hotta Y, et al. (2009) Fibroblast growth factor 21 regulates lipolysis in white adipose tissue but is not required for ketogenesis and triglyceride clearance in liver. *Endocrinology* 150:4625–4633.
24. Potthoff MJ, et al. (2009) FGF21 induces PGC-1alpha and regulates carbohydrate and fatty acid metabolism during the adaptive starvation response. *Proc Natl Acad Sci USA* 106:10853–10858.
25. Shimada T, et al. (2004) Targeted ablation of Fgf23 demonstrates an essential physiological role of FGF23 in phosphate and vitamin D metabolism. *J Clin Invest* 113: 561–568.
26. Powers CJ, McLeskey SW, Wellstein A (2000) Fibroblast growth factors, their receptors and signaling. *Endocr Relat Cancer* 7:165–197.
27. Yu C, et al. (2000) Elevated cholesterol metabolism and bile acid synthesis in mice lacking membrane tyrosine kinase receptor FGFR4. *J Biol Chem* 275:15482–15489.
28. Berglund ED, et al. (2009) Fibroblast growth factor 21 controls glycemia via regulation of hepatic glucose flux and insulin sensitivity. *Endocrinology* 150:4084–4093.
29. Xu J, et al. (2009) Fibroblast growth factor 21 reverses hepatic steatosis, increases energy expenditure, and improves insulin sensitivity in diet-induced obese mice. *Diabetes* 58:250–259.
30. Kurosu H, et al. (2006) Regulation of fibroblast growth factor-23 signaling by klotho. *J Biol Chem* 281:6120–6123.
31. Kolek OI, et al. (2005) 1alpha,25-Dihydroxyvitamin D3 upregulates FGF23 gene expression in bone: The final link in a renal-gastrointestinal-skeletal axis that controls phosphate transport. *Am J Physiol Gastrointest Liver Physiol* 289:G1036–G1042.
32. Inagaki T, et al. (2007) Endocrine regulation of the fasting response by PPARalpha-mediated induction of fibroblast growth factor 21. *Cell Metab* 5:415–425.
33. Badman MK, et al. (2007) Hepatic fibroblast growth factor 21 is regulated by PPARalpha and is a key mediator of hepatic lipid metabolism in ketotic states. *Cell Metab* 5:426–437.

Adipose Tissue–Specific Regulation of Angiotensinogen in Obese Humans and Mice: Impact of Nutritional Status and Adipocyte Hypertrophy

Shintaro Yasue[1], Hiroaki Masuzaki[1], Sadanori Okada[1], Takako Ishii[1], Chisayo Kozuka[1], Tomohiro Tanaka[1], Junji Fujikura[1], Ken Ebihara[1], Kiminori Hosoda[1], Akemi Katsurada[2], Naro Ohashi[2], Maki Urushihara[2], Hiroyuki Kobori[2], Naoki Morimoto[3], Takeshi Kawazoe[3], Motoko Naitoh[3], Mitsuru Okada[4], Hiroshi Sakaue[4,5], Shigehiko Suzuki[3] and Kazuwa Nakao[1]

BACKGROUND

The adipose tissue renin–angiotensin system (RAS) has been implicated in the pathophysiology of obesity and dysfunction of adipose tissue. However, neither regulation of angiotensinogen (AGT) expression in adipose tissue nor secretion of adipose tissue–derived AGT has been fully elucidated in humans.

METHODS

Human subcutaneous abdominal adipose tissue (SAT) biopsies were performed for 46 subjects with a wide range of body mass index (BMI). Considering the mRNA level of AGT and indices of body fat mass, the amount of adipose tissue–derived AGT secretion (A-AGT-S) was estimated. Using a mouse model of obesity and weight reduction, plasma AGT levels were measured with a newly developed enzyme-linked immunosorbent assay (ELISA), and the contribution of A-AGT-S to plasma AGT levels was assessed.

RESULTS

A-AGT-S was substantially increased in obese humans and the value was correlated with the plasma AGT level in mice. A-AGT-S and plasma AGT were higher in obese mice, whereas lower in mice with weight reduction. However, the AGT mRNA levels in the liver, kidney, and aorta were not altered in the mouse models. In both humans and mice, the AGT mRNA levels in mature adipocytes (MAs) were comparable to those in stromal-vascular cells. Coulter Multisizer analyses revealed that AGT mRNA levels in the MAs were inversely correlated with the average size of mature adipocytes.

CONCLUSIONS

This study demonstrates that adipose tissue–derived AGT is substantially augmented in obese humans, which may contribute considerably to elevated levels of circulating AGT. Adipose tissue–specific regulation of AGT provides a novel insight into the clinical implications of adipose tissue RAS in human obesity.

Keywords: *adipocyte size; adipose tissue; angiotensinogen; blood pressure; hypertension; obesity*

Am J Hypertens 2010; **23**:425-431 © 2010 American Journal of Hypertension, Ltd.

Activation of the renin–angiotensin system (RAS) is commonly observed in patients with obesity.[1,2] Angiotensin-converting enzyme (ACE) inhibitors and angiotensin II type 1 receptor (AT1R) blockers ameliorate obesity-related metabolic derangement.[3,4] Of note, Case-J trial demonstrated that a systemic blockade of RAS significantly reduced the incidence of newly occurring type 2 diabetes, notably in obese patients with hypertension.[5] Adipose tissue expresses all components of RAS (angiotensinogen (AGT), renin, ACE, AT1R, and angiotensin II type 2 receptor (AT2R)) in humans and rodents,[1] implicating adipose tissue RAS in the pathophysiology of obesity.

AGT, the only substrate of renin, is expressed in a variety of tissues.[1,2] Besides the liver, adipose tissue has recently been recognized as a considerable source of AGT.[1] A previous study demonstrated that transgenic overexpression of AGT exclusively in adipose tissue augmented circulation level of AGT and rescued hypotension and leanness seen in AGT knockout mice.[6] This observation indicates that adipose tissue–derived AGT contributes to circulating AGT level and resultant pathophysiology

[1]Department of Medicine and Clinical Science, Kyoto University Graduate School of Medicine, Kyoto, Japan; [2]Department of Physiology, and Hypertension and Renal Center of Excellence, Tulane University Health Sciences Center, New Orleans, Louisiana, USA; [3]Department of Plastic and Reconstructive Surgery, Kyoto University Graduate School of Medicine, Kyoto, Japan; [4]Division of Diabetes, Digestive, and Kidney Diseases, Department of Clinical Molecular Medicine, Kobe University Graduate School of Medicine, Kobe, Japan; [5]Department of Pharmacology, Kinki University School of Medicine, Sayama, Japan. Correspondence: Hiroaki Masuzaki (hiroaki@kuhp.kyoto-u.ac.jp)

Received 13 September 2009; first decision 3 November 2009; accepted 4 December 2009; advance online publication 7 January 2010. doi:10.1038/ajh.2009.263

of obesity-related metabolic diseases. Although some recent studies demonstrated that expression of adipose AGT is modified by adiposity in humans and rodents,[1,7,8] secretion of adipose tissue–derived AGT *per se* has not been elucidated. Therefore, the extent to which adipose tissue–derived AGT secretion (A-AGT-S) contributes to plasma AGT levels has not been clarified.

In this context, this study was designed to estimate the amount of A-AGT-S, considering the mRNA level of AGT and indices of body fat mass, and explored the potential regulation of A-AGT-S in relation to obesity by performing human adipose tissue biopsies. Furthermore, plasma AGT levels were measured using a newly developed enzyme-linked immunosorbent assay (ELISA),[9,10] and the contribution of A-AGT-S to plasma AGT in mouse models of obesity and weight reduction was assessed.

Although the mechanistic link between adipocyte size and metabolic consequences has long been of research interest,[11,12] the relationship between adipocyte hypertrophy and the expression level of AGT in adipocytes was not fully investigated in humans. Most of the previous studies have employed a histological approach for evaluating adipocyte size.[8,11] However, the distribution of adipocyte diameter is bimodal in humans,[12,13] resulting in limitations in assessing the representative size of adipocytes. In this context, size of mature adipocytes was precisely analyzed using a Coulter Multisizer,[12] and the possible relationship between adipocyte size and AGT mRNA level in adipocytes was explored in humans.

METHODS

Profile of subjects. This study was approved by the ethical committee on human research of Kyoto University Graduate School of Medicine (no. 553). Signed informed consent was obtained from all subjects. A total of 46 Japanese subjects (**Table 1**: 24 men and 22 women; body mass index (BMI): 29 ± 1.0 kg/m^2) were recruited for subcutaneous abdominal adipose tissue (SAT) biopsies. Patients who had received ACE inhibitors, AT1R blockers, thiazolidinediones, insulin, or steroid-related drugs were carefully excluded. Among the group, the serum leptin level was measured in 39 subjects (20 men and 19 women; BMI: 28 ± 1.2 kg/m^2). To examine the relationship between body fat mass and serum leptin level, 55 subjects (BMI: 27 ± 2.1 kg/m^2, range: 15–52) were recruited during the same period.

SAT biopsies. Adipose tissue biopsies were performed before controlling calorie intake and physical activity. SAT (~2 g) was removed from the periumbilical region under local anesthesia (lidocaine 1%). Samples were frozen in liquid nitrogen immediately and stored at −80 °C for total RNA extraction.

Hormone assays and clinical parameters. Blood samples were obtained at 0800 hours after an overnight fast 3 days before the adipose tissue biopsies. Serum leptin levels were measured using RIA (LINCO Research, St Louis, MO).

Real-time PCR. Total RNA was extracted using a QIAGEN RNeasy Kit (QIAGEN Japan, Tokyo, Japan). Complementary DNA was synthesized using an iScript cDNA Synthesis Kit (Bio-Rad, Hercules, CA). The mRNA level was quantified using the TaqMan PCR method with an ABI PRISM 7700 Sequence Detection System (Applied Biosystems, Foster City, CA).[14] The sequences of primers and probes for each gene are summarized in **Table 2**. Values were normalized to that of 18S rRNA (Applied Biosystems).

Obese and weight-losing mouse models. In diet-induced obese (12W DIO, $n = 6$) model experiments, 8-week-old male C57BL/6J mice were housed for 4 weeks on a high-fat/high-sucrose diet (D12493; Oriental Bio-Service, Kyoto, Japan) or regular diet (12W RD, $n = 6$) (F-2; Funahashi, Chiba, Japan). In the weight-losing (14W WL) mouse experiments, 6-week-old male C57BL/6J mice were maintained on a high-fat/high-sucrose diet for 4 weeks, then from 10 weeks of age were subjected to diet substitution from a high-fat/high-sucrose diet to an RD for 4 weeks. In addition, 6-week-old male C57BL/6J mice were maintained on high-fat/high-sucrose diet (14W DIO, $n = 6$) for 8 weeks. Experimental protocol of obese and weight-losing mouse models is schematized in **Supplementary Figure S1** online.

Estimation of A-AGT-S. The amount of A-AGT-S was estimated by multiplying the mRNA level of AGT/g adipose tissue with the weight of body fat mass. Because serum leptin level was tightly correlated with body fat mass,[15] the serum leptin levels were used as a representative index of body fat mass in humans. Estimation of A-AGT-S is schematized in **Supplementary Figure S2** online.

ELISA for AGT. AGT protein was determined using a newly developed ELISA.[9,10]

Cell culture. 3T3–L1 fibroblasts were maintained and differentiated into mature adipocytes.[14] Fully differentiated adipocytes (day 8) were exposed to 10^{-9}, 10^{-8}, or 10^{-7} mol/l dexamethasone for 48 h. Total RNA was extracted from cultured cells using TRIzol Reagent (Invitrogen, Carlsbad, CA). For protein extraction, tissue was homogenized in a radioimmune precipitation (Upstate Cell Signaling Solutions, New York, NY)

Table 1 | Profile of subjects

	n	Mean ± s.e.m.	Range
Age (years)	46	46 ± 2.1	20–74
BMI (kg/m^2)	46	29 ± 1.0	18–52
Waist circumference (cm)	46	93 ± 2.5	63–141
Serum leptin (ng/ml)	39	15 ± 2.2	1.7–68
SBP (mm Hg)	46	131 ± 2.7	94–200
DBP (mm Hg)	46	79 ± 1.5	55–108

BMI, body mass index; DBP, diastolic blood pressure; SBP, systolic blood pressure.

Table 2 | Oligonucleotide sequences for primers and probes

Gene	Forward/reverse primer Probe
Human AGT	5′GGTGGAGGGTCTCACTTTCCA3′/5′ATGGTCAGGTGGATGGTCCG3′ 5′CCCTCAACTGGATGAAGAAACTGTCTCC3′
Human renin	5′GCTATTCAACAGGGACAGTCAG3′/5′TCCGTGACCTCTCCAAACATC3′ 5′AGCCAGGACATCATCACCGTGGGT3′
Human ACE	5′TGCACAGTCTCAACCTGCTG3′/5′CAAGGGCCATCTTCATCAGAAAG3′ 5′TCAGCAGCTCCTAGTTCTTATGCCTTTGGT3′
Human AT1R	5′GGGGCGCGGGTGTATTTG3′/5′TTCAGTAGAAGAGTTGAGAATCATTTTG3′ 5′AGTGTTTGCAACAAATTCGACCCAGGTGA3′
Human AT2R	5′GCTGATTTATGATAACTGCTTTAAACTTC3′/5′GGTGGAGTTGCCCTTCATATTG3′ 5′TCAGCAGCTCCTAGTTCTTATGCCTTTGGT3′
Human adiponectin	5′CCGTGATGGCAGAGATGGCA3′/5′TGAGAAGGGTGAGAAAGGAGATCCAGGT3′ 5′CCGATGTCTCCCTTAGGACCAAT3′
Mice AGT	5′ACACCTACGTTCACTTCCAAG3′/5′CCGAGATGCTGTTGTCCAC3′ 5′ATGAGAGGTTTCTCTCAGCTGCCTGGA3′
Mice renin	5′GCTCCCTGAAGTTGATCATGC3′/5′GTGGGCACCTGGCTACAG3′ 5′CTCTTCTCCTTGGCTCCCAGGGCT3′
Mice ACE	5′TCCCAAAGTATGTGGAGTTCTCC3′/5′TTGTCAGACTCGTATAAGGATCTCC3′ 5′CCCTGCATCCGTGTAGCCATTGAGC3′
Mice AT1aR	5′TACCAGCTCTGCGGCTCTC3′/5′TGCTGTGAGTTATCCAGACAAAATG3′ 5′AGCTCTGCTGCTCTCCCGGACTTAAC3′
Mice AT2R	5′GATGGAGGGAGCTCGGAAC3′/5′TTTAAAGCAGTTATCATAAATCAGCTTAC3′ 5′CACTCCTTAAAATGCAGGCTGAAGTAAGCT3′

The sequences of primers and probes for each gene used in this study are summarized.
AGT, angiotensinogen; ACE, angiotensin-converting enzyme; AT1R, angiotensin II type 1 receptor; AT1aR, angiotensin II type 1a receptor; AT2R, angiotensin II type 2 receptor.

buffer containing protease inhibitors (Complete; Roche, Basel, Switzerland).

Measurement of adipocyte diameter by a Coulter Multisizer. A total of 15 human subjects (5 men and 10 women; age: 51 ± 3.8 years; BMI: 28 ± 2.5 kg/m^2) were analyzed. Stromal-vascular cells and mature adipocytes (MAs) were isolated.[16] Adipocyte size was determined by a Beckman Coulter Multisizer III (Beckman Coulter, High Wycombe, UK).[12] Approximately 8,000 cells were analyzed using a Coulter Multisizer equipped with a 560-μm aperture tube. After collection of pulse sizes, data were expressed as particle diameters and displayed as histograms of counts against diameter, using linear bins and a linear scale for the *x*-axis.[12]

Statistical analyses. Values are expressed as mean ± s.e.m. Values not distributed normally were transformed into a logarithmic (natural logarithm) distribution and were analyzed using Pearson's correlation coefficient. A Student's *t*-test was used to compare the data (Social Research Information, Tokyo, Japan).

RESULTS

AGT mRNA expression and protein synthesis in 3T3-L1 adipocytes and human adipose tissue

Level of mRNA and protein of AGT were measured in lysates and cultured media in 3T3-L1 adipocytes treated with 10^{-9}, 10^{-8}, or 10^{-7} mol/l dexamethasone for 24 h. AGT protein level in lysates and cultured media were strongly correlated with the AGT mRNA level ($r = 0.98$, $P < 0.01$) (see **Supplementary Figure S3a** online) ($r = 0.84$, $P < 0.01$) (see **Supplementary Figure S3b** online).

Relationship between AGT protein/g adipose tissue and AGT mRNA levels in human SAT was also explored ($n = 7$, BMI: 29 ± 0.4 kg/m^2, range 19–48). Consistent with the results in 3T3-L1 adipocytes, AGT protein/g adipose tissue was correlated with the AGT mRNA level in human adipose tissue ($r = 0.77$, $P = 0.04$) (see **Supplementary Figure S3c** online).

Impact of adipose tissue-derived AGT secretion on obesity and blood pressure in humans

The mRNA levels of RAS genes, AGT, renin, ACE, AT1R, and AT2R in human SAT were analyzed. The AGT mRNA level was inversely correlated with BMI ($r = -0.32$, $P = 0.02$) (**Figure 1a**). On the other hand, no correlation was observed between the ACE mRNA level and BMI ($r = 0.08$, $P = 0.63$). The AT1R mRNA level was inversely correlated with BMI ($r = -0.32$, $P = 0.02$). Renin and AT2R mRNA levels were undetectable. The mRNA level of adiponectin was analyzed. No significant correlations were observed between adiponectin mRNA level and BMI ($r = 0.08$, $P = 0.56$) or AGT mRNA level ($r = 0.09$, $P = 0.49$). We also focused our attention on the possibilities of gender differences in AGT gene expression. When divided into two groups (BMI >25 (obese) and BMI <25 (lean)), the differences of AGT mRNA levels by gender were not observed in lean (male $n = 9$:female $n = 12$) and obese (male $n = 15$: female $n = 10$).

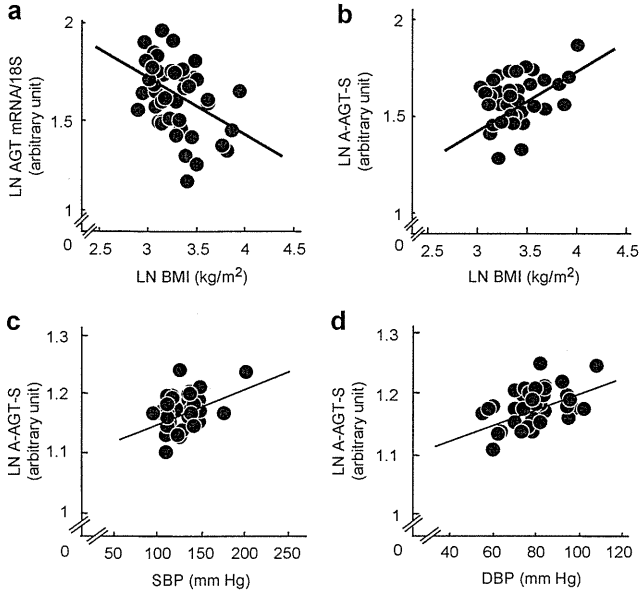

Figure 1 | Impact of adipose tissue–derived AGT secretion on obesity and blood pressure in humans. (**a**) Relation between AGT mRNA level and BMI ($n = 46$). (**b**) Relationship between adipose tissue–derived AGT secretion (A-AGT-S) and BMI ($n = 39$). (**c**) Relationship between A-AGT-S and systolic blood pressure (SBP) ($n = 39$). (**d**) Relationship between A-AGT-S and diastolic blood pressure (DBP) ($n = 39$). AGT, angiotensinogen; BMI, body mass index; LN, natural logarithm.

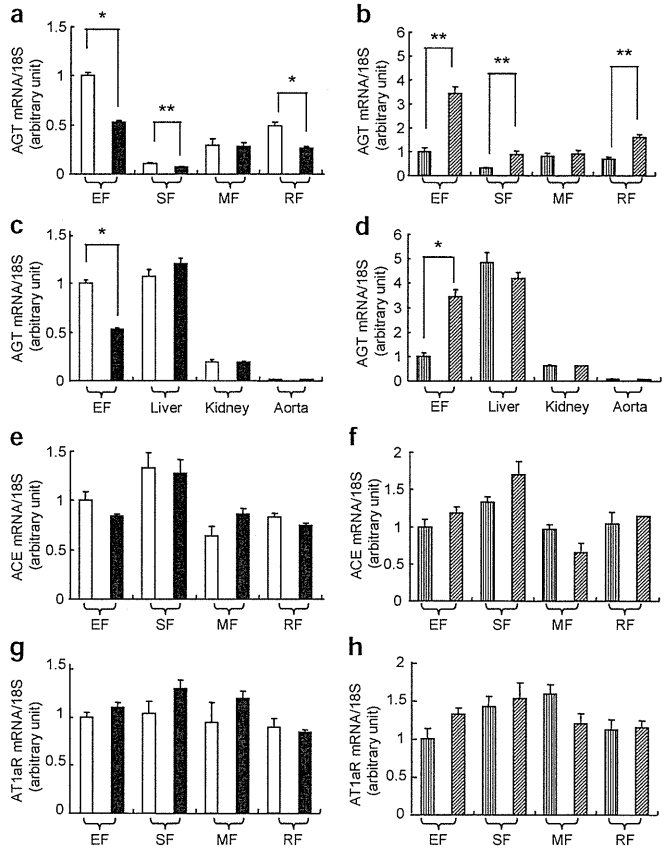

Figure 2 | Expression of genes involved in renin–angiotensin system in obese and weight-losing mouse. AGT mRNA levels in (**a**) 12W RD ($n = 6$) and 12W DIO ($n = 6$) and in (**b**) 14W DIO ($n = 6$) and 14W WL ($n = 6$) in epididymal fat (EF), subcutaneous fat (SF), mesenteric fat (MF), and retroperitoneal fat (RF). AGT mRNA levels in (**c**) 12W RD and 12W DIO and in (**d**) 14W DIO and 14W WL in the liver, kidney, and aorta. ACE mRNA levels in (**e**) 12W RD and 12W DIO and in (**f**) 14W DIO and 14W WL. AT1aR mRNA levels in (**g**) 12W RD and 12W DIO and in (**h**) 14W DIO and 14W WL. White bar, 12W RD; black bar, 12W DIO; vertical striping bar, 14W DIO; diagonal striping bar, 14W WL. $^*P < 0.01$, $^{**}P < 0.05$. ACE, angiotensin-converting enzyme; AGT, angiotensinogen; AT1aR, angiotensin II type 1a receptor; DIO, diet-induced obesity; WL, weight-losing.

Based on the results that AGT is secreted constitutively (see **Supplementary Figure S3a–c** online), AGT mRNA expression was predicted to parallel the AGT secretion. In this context, the amount of A-AGT-S was estimated by multiplying the mRNA level of AGT/g adipose tissue with serum leptin, a representative index of body fat mass. The serum leptin level in 55 subjects was correlated with body fat mass ($r = 0.76$, $P = 0.00000000001$). Contrary to AGT mRNA level, A-AGT-S was correlated with BMI ($n = 39$, $r = 0.36$, $P = 0.02$) (**Figure 1b**). A-AGT-S was correlated with systolic blood pressure ($n = 39$, $r = 0.36$, $P = 0.02$) (**Figure 1c**) and diastolic blood pressure ($n = 39$, $r = 0.45$, $P < 0.01$) (**Figure. 1d**). In both male group ($n = 20$) and female group ($n = 19$), A-AGT-S was correlated with BMI, systolic blood pressure, and diastolic blood pressure (data not shown).

Expression of genes involved in the RAS in obese and weight-losing mouse models

The mRNA levels of RAS genes were analyzed in obese and weight-losing mouse models described in Methods. The AGT mRNA levels in epididymal fat (EF), subcutaneous fat (SF), and retroperitoneal fat (RF) were lower in 12W DIO than in 12W RD (**Figure 2a**). In contrast, the AGT mRNA levels in EF, SF, and RF were elevated in 14W WL (**Figure 2b**). In the liver, kidney, and aorta, all of which are recognized as AGT-producing organs,[2] the AGT mRNA levels were equivalent between 12W DIO and 12W RD, or between 14W WL and 14W DIO (**Figure 2c,d**). Levels of ACE and angiotensin II type 1a receptor (AT1aR) mRNA in EF, SF, mesenteric fat (MF), and RF were also equivalent between 12W DIO and 12W RD or between 14W WL and 14W DIO (ACE: **Figure 2e,f**) (AT1aR: **Figure 2g,h**). AGT was decreased, although other genes involving RAS did not vary, in adipose tissue from the genetically obese *ob/ob* mice (data not shown).

Adipose tissue–derived AGT secretion and plasma AGT levels in obese and weight-losing mouse models

To assess the secretion of AGT from adipose tissue in body weight change, the amounts of A-AGT-S in obese and weight-losing mice were estimated by multiplying the AGT mRNA level/g adipose tissue with the weight of EF, SF, MF, or RF. The weights of EF, SF, MF, and RF in 12W DIO were increased ~3.5-fold in comparison with 12W RD, whereas the weights of EF, SF, MF, and RF in 14W WL were decreased by one-third compared to 14W DIO. Under caloric intervention, changes in weights in the liver and kidney were subtle compared to fat depots (~20% in liver and ~5% in kidney). A-AGT-S in EF, SF, MF, and RF was significantly increased

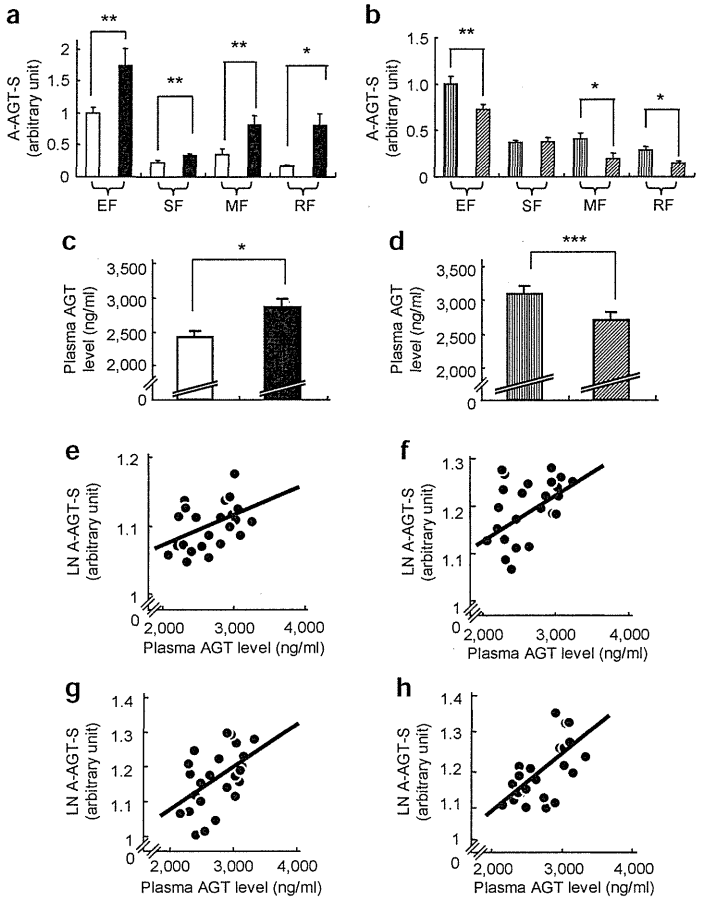

Figure 3 | Adipose tissue–derived AGT secretion and plasma AGT level between obese and weight-losing mouse. Adipose tissue–derived AGT secretion (A-AGT-S) in (**a**) 12W RD ($n = 6$) and 12W DIO ($n = 6$) and in (**b**) 14W DIO ($n = 6$) and 14W WL ($n = 6$) in epididymal fat (EF), subcutaneous fat (SF), mesenteric fat (MF), and retroperitoneal fat (RF). Plasma AGT levels in (**c**) 12W RD and 12W DIO and in (**d**) 14W DIO and 14W WL. Relationship between A-AGT-S and plasma AGT levels in (**e**) EF, (**f**) SF, (**g**) MF, and (**h**) RF. White bar, 12W RD; black bar, 12W DIO; vertical striping bar, 14W DIO; diagonal striping bar, 14W WL. $^*P < 0.01$, $^{**}P < 0.05$, $^{***}P = 0.05$. AGT, angiotensinogen; DIO, diet-induced obesity; LN, natural logarithm; WL, weight-losing.

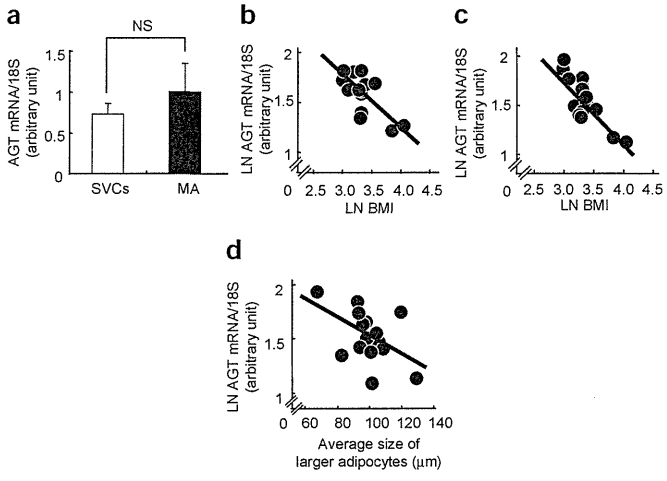

Figure 4 | Relationship between cell size and AGT mRNA level in isolated mature adipocytes in humans. (**a**) AGT mRNA level in stromal-vascular cells (SVCs) and mature adipocytes (MAs) isolated from human subcutaneous abdominal adipose tissue (SAT) ($n = 15$; BMI: 28 ± 2.5 kg/m^2). White bar, SVCs; black bar, MAs. Relationship between BMI and the AGT mRNA level in (**b**) SVCs or (**c**) MAs isolated from human SAT. (**d**) Relationship between the AGT mRNA level in MAs and the average size of large adipocytes in human SAT ($n = 15$; BMI: 28 ± 2.5 kg/m^2). AGT, angiotensinogen; LN, natural logarithm.

in 12W DIO compared to 12W RD (**Figure 3a**). In contrast, A-AGT-S in EF, MF, and RF was decreased in 14W WL compared to 14W DIO (**Figure 3b**). To further explore the impact of obesity on circulating AGT, plasma AGT levels were measured in 12W DIO, 12W RD, 14W WL, and 14W DIO using a newly developed ELISA.[10] The plasma AGT level was elevated in 12W DIO ($2{,}884 \pm 118$ ng/ml) compared to 12W RD ($2{,}431 \pm 85$ ng/ml) (**Figure 3c**). In contrast, the plasma AGT level in 14W WL ($2{,}703 \pm 116$ ng/ml) was lower than in 14W DIO ($3{,}088 \pm 133$ ng/ml) (**Figure 3d**). A-AGT-S in EF, SF, MF, and RF were correlated with plasma AGT level in mouse of obesity and weight reduction (EF: $r = 0.49$, $P < 0.01$ (**Figure 3e**); SF: $r = 0.43$, $P = 0.02$ (**Figure 3f**); MF: $r = 0.41$, $P = 0.03$ (**Figure 3g**); RF: $r = 0.64$, $P < 0.01$ (**Figure 3h**)).

Relationship between cell size and AGT mRNA level in isolated mature adipocytes in humans

To investigate the potential link between adipocyte size and the mRNA level of AGT in isolated MAs, adipocyte size was measured using a Coulter Multisizer[12] in human SAT ($n = 15$; BMI: 28 ± 2.5 kg/m^2, range: 19–55). The AGT mRNA level in MAs was comparable to that in stromal-vascular cells (**Figure 4a**).

The levels of AGT in stromal-vascular cells and MAs were inversely correlated with BMI ($r = -0.69$, $P < 0.01$ (**Figure 4b**), $r = -0.84$, $P < 0.01$ (**Figure 4c**). Consistent with a previous report,[12] the size distribution of adipocytes displayed as histograms against diameters was bimodal in all cases. The nadir was defined as the low point between the large adipocytes and small adipocytes.[12] BMI was positively correlated with both nadir size and average size of the larger adipocytes ($r = 0.50$, $P < 0.05$; $r = 0.48$, $P < 0.05$, respectively). The AGT mRNA level in isolated MA was inversely correlated with the average size of the larger adipocytes ($r = -0.48$, $P < 0.05$ (**Figure 4d**).

DISCUSSION

The primary findings of this study are (i) A-AGT-S was substantially increased in both obese humans and obese mice. (ii) A-AGT-S was correlated with plasma AGT level in mouse models of obesity and weight reduction. A-AGT-S and plasma AGT were increased in obese mice, while decreased in mice with weight reduction. (iii) The AGT mRNA level in adipose tissue was decreased in both obese humans and mice, but increased in mice with weight reduction. The AGT mRNA levels in the liver, kidney, and aorta were not altered in mouse models of obesity and weight reduction. In contrast, expression of genes involved in RAS other than AGT did not change in adipose tissue from obese and weight-losing mice. (iv) AGT was secreted constitutively from adipocytes and adipose tissue in both humans and mice. (v) Coulter Multisizer analyses revealed that the AGT mRNA level in MAs was correlated inversely with the average size of adipocytes larger than the nadir of bimodal histograms.

As AGT is secreted from many organs including liver, kidney, and vascular cells,[1,2] contribution of adipose tissue to plasma AGT level has not been determined. Furthermore, precise measurements of plasma AGT level were not conducted; instead, the radioimmunoassay result for angiotensin I has long been used as an equivalent.[1,17] In this context, an accurate assessment of A-AGT-S is critical for investigating clinical implications of adipose tissue RAS. Using a newly developed ELISA.[9,10] this study demonstrated for the first time that AGT was secreted constitutively from adipocytes and adipose tissue (**Supplementary Figures S3** online). Based on our novel finding, A-AGT-S was estimated by multiplying the mRNA level of AGT/g adipose tissue and fat mass or serum leptin, where applicable. Notably, only AGT is nutritionally regulated in adipose tissue from mice among RAS components (**Figure 2a,b,e–h**) reinforcing the rationale for focusing on A-AGT-S.

In this study, plasma AGT levels were increased ~20% in the obese mouse, whereas they were decreased ~12% in mice with weight reduction. A-AGT-S in EF, SF, MF, and RF was correlated with plasma AGT (**Figure 3e–h**). In contrast, AGT mRNA levels in the liver, kidney, and aorta were not altered in body weight changes (**Figure 2c,d**), suggesting adipose tissue–specific regulation of AGT in obesity. Under caloric intervention, changes in weights in the liver and kidney were subtle compared to fat depots, supporting the notion that AGT from the liver and kidney may not vary considerably in obesity or weight reduction. Taken together, it is reasonable to speculate that A-AGT-S contributes considerably (~20%) to plasma AGT level, accompanied by an increase in body fat mass.

Nevertheless the notion that visceral fat contributes to only ~10% of total adipose tissue mass in nonobese humans,[18] visceral adipose tissue–derived AGT secretion would not be negligible. In this context, in mouse models, we analyzed A-AGT-S in EF, MF, and RF, in addition to SF. A-AGT-S in EF, MF, and RF was increased in obese mice, whereas decreased in mice with weight reduction, and the A-AGT-S value in each adipose depot was correlated with plasma AGT level. Based on these results, it is likely to speculate that visceral adipose tissue–derived AGT secretion, like subcutaneous adipose tissue–derived AGT secretion, is substantially augmented and contributes to the plasma AGT level in human obesity.

Adipose tissue AGT mRNA levels were decreased by obesity and increased by weight loss, whereas A-AGT-S showed the opposite trend (**Figures 1–3**). It is likely that increased mass of adipose tissue in obesity overwhelmed the decrease in AGT expression, resulting in an increase in A-AGT-S and plasma AGT. Increased leptin mRNA level contributes to the extreme elevation of plasma leptin level in obesity.[19] Distinct from leptin, it is reasonable to speculate that AGT mRNA in adipose tissue is regulated so that plasma AGT concentration does not rise extremely in obesity. Although a series of hormonal and inflammatory changes may control AGT expression in adipose tissue,[1,20] the mechanism whereby AGT mRNA level is decreased exclusively in obese adipose tissue still remains obscure.

The mechanistic link between adipocyte size and metabolic consequences has long stimulated great interest in research.[11,12] To date, most of studies have employed histological analyses for assessing adipocyte size.[8,11] However, it should be noted that the distribution of adipocyte diameter is bimodal in humans.[12,13] Therefore, in this study, adipocyte size was analyzed using a Coulter Multisizer, which allows determination of the distribution of adipocyte size with greatest accuracy.[12] The progression of obesity is tightly associated with adipocyte hypertrophy.[21] In agreement with this notion, the average size of adipocytes larger than the nadir[12] was correlated with BMI ($r = 0.51$, $P = 0.03$), indicating that an increase in the average size of larger adipocytes tightly reflects adipocyte hypertrophy. The AGT mRNA level in isolated MAs was inversely correlated with the average size of larger adipocytes in humans (**Figure 4d**). We recently found that the AGT mRNA level was decreased in a long-term culture (~28 days) of 3T3–L1 adipocytes, with a concomitant increase in cellular triglyceride content (S. Okada, C. Kozuka, H. Masuzaki, S. Yasue, T. Ishii-Yonemato, Y. Yamamoto, M. Noguchi, T. Kusakabe, T. Tomita, J. Fujikura, K. Ebihara, K. Hosoda, H. Sakaue, H. Kobori, M. Ham, Y. Sok Lee, J. Bum Kim, Y. Saito, and K. Nakao, unpublished data). Although further studies are warranted, triglyceride accumulation and adipocyte hypertrophy may contribute to a decrease in AGT mRNA expression in obese adipose tissue.

In summary, this study is the first to demonstrate that secretion of adipose tissue–derived AGT is substantially augmented and contributes to the plasma AGT level in both obese humans and obese mice. Our results suggest that increase in adipose tissue–derived AGT contributes to circulating AGT level and resultant pathophysiology of obesity-related metabolic diseases.

Supplementary material is linked to the online version of the paper at http://www.nature.com/ajh

Acknowledgments: We are grateful to Mrs A. Ryu, S. Maki, and Ms. M. Nagamoto for assistance. This work was supported in part by a Grant-in-Aid for Scientific Research (B2), Takeda Medical Research Foundation, and Lilly Research Foundation. Clinical Trial Registration Number: UMIN000001969.

Disclosure: The authors declared no conflict of interest.

1. Engeli S, Schling P, Gorzelniak K, Boschmann M, Janke J, Ailhaud G, Teboul M, Massiéra F, Sharma AM. The adipose-tissue renin-angiotensin-aldosterone system: role in the metabolic syndrome? *Int J Biochem Cell Biol* 2002; 35: 807–825.
2. Dzau VJ. Circulating versus local renin-angiotensin system in cardiovascular homeostasis. *Circulation* 1988; 77:4–13.
3. Kurtz TW. Beyond the classic angiotensin-receptor-blocker profile. *Nat Clin Pract Cardiovasc Med* 2008; 5 Suppl 1:S19–S26.
4. Yusuf S, Sleight P, Pogue J, Bosch J, Davies R, Dagenais G. Effects of an angiotensin-converting-enzyme inhibitor, ramipril, on cardiovascular events in high-risk patients. The Heart Outcomes Prevention Evaluation Study Investigators. *N Engl J Med* 2000; 20:145–153.
5. Ogihara T, Nakao K, Fukui T, Fukiyama K, Saruta T. Clinical outcomes in hypertensive patients with high cardiovascular risks: principal results of candesartan antihypertensive survival evaluation in Japan (CASE-J) study. In: The 21st Scientific Meeting of the International Society of Hypertension, Fukuoka, Japan, 2006.
6. Massiera F, Bloch-Faure M, Ceiler D, Murakami K, Fukamizu A, Gasc JM, Quignard-Boulange A, Negrel R, Ailhaud G, Seydoux J, Meneton P, Teboul M. Adipose angiotensinogen is involved in adipose tissue growth and blood pressure regulation. *FASEB J* 2001; 15:2727–2729.
7. Giacchetti G, Faloia E, Mariniello B, Sardu C, Gatti C, Camilloni MA, Guerrieri M, Mantero F. Overexpression of the renin-angiotensin system in human visceral adipose tissue in normal and overweight subjects. *Am J Hypertens* 2002; 15:381–388.
8. Hainault I, Nebout G, Turban S, Ardouin B, Ferre P, Quignard-Boulange A. Adipose tissue-specific increase in angiotensinogen expression and secretion in the obese (fa/fa) Zucker rat. *Am J Physiol Endocrinol Metab* 2002; 282:E59–E66.
9. Katsurada A, Hagiwara Y, Miyashita K, Satou R, Miyata K, Ohashi N, Navar LG, Kobori H. Novel sandwich ELISA for human angiotensinogen. *Am J Physiol Renal Physiol* 2007; 293:F956–F960.
10. Kobori H, Katsurada A, Miyata K, Ohashi N, Satou R, Saito T, Hagiwara Y, Miyashita K, Navar LG. Determination of plasma and urinary angiotensinogen levels in rodents by newly developed ELISA. *Am J Physiol Renal Physio* 2008; 294: F1257–F1263.
11. Jernås M, Palming J, Sjöholm K, Jennische E, Svensson PA, Gabrielsson BG, Levin M, Sjögren A, Rudemo M, Lystig TC, Carlsson B, Carlsson LM, Lönn M. Separation of human adipocytes by size: hypertrophic fat cells display distinct gene expression. *FASEB J* 2006; 20:1540–1542.
12. McLaughlin T, Sherman A, Tsao P, Gonzalez O, Yee G, Lamendola C, Reaven GM, Cushman SW. Enhanced proportion of small adipose cells in insulin-resistant vs insulin-sensitive obese individuals implicates impaired adipogenesis. *Diabetologia* 2007; 50:1707–1715.
13. Julien P, Despres JP, Angel A. Scanning electron microscopy of very small fat cells and mature fat cells in human obesity. *J Lipid Res* 1989; 30:293–299.
14. Arai N, Masuzaki H, Tanaka T, Ishii T, Yasue S, Kobayashi N, Tomita T, Noguchi M, Kusakabe T, Fujikura J, Ebihara K, Hirata M, Hosoda K, Hayashi T, Sawai H, Minokoshi Y, Nakao K. Ceramide and adenosine 5′-monophosphate-activated protein kinase are two novel regulators of 11β-hydroxysteroid dehydrogenase type 1 expression and activity in cultured preadipocytes. *Endocrinology* 2007; 148:5268–5277.
15. Friedman JM, Halaas JL. Leptin and the regulation of body weight in mammals. *Nature* 1998; 395:763–770
16. Masuzaki H, Ogawa Y, Isse N, Satoh N, Okazaki T, Shigemoto M, Mori K, Tamura N, Hosoda K, Yoshimasa Y, Jingami H, Kawada T, Nakao K. Human obese gene expression. Adipocyte-specific expression and regional differences in the adipose tissue. *Diabetes* 1995; 44:855–858.
17. Umemura S, Nyui N, Tamura K, Hibi K, Yamaguchi S, Nakamaru M, Ishigami T, Yabana M, Kihara M, Inoue S, Ishii M. Plasma angiotensinogen concentrations in obese patients. *Am J Hypertens* 1997; 10:629–633.
18. Wajchenberg BL. Subcutaneous and visceral adipose tissue: their relation to the metabolic syndrome. *Endocr Rev* 2000; 21:697–738
19. Lönnqvist F, Nordfors L, Jansson M, Thörne A, Schalling M, Arner P. Leptin secretion from adipose tissue in women. Relationship to plasma levels and gene expression. *J Clin Inves* 1997; 99:2398–2404.
20. Aubert J, Darimont C, Safonova I, Ailhaud G, Negrel R. Regulation by glucocorticoids of angiotensinogen gene expression and secretion in adipose cells. *Biochem J* 1997; 328:701–706.
21. Bays HE, González-Campoy JM, Bray GA, Kitabchi AE, Bergman DA, Schorr AB, Rodbard HW, Henry RR. Pathogenic potential of adipose tissue and metabolic consequences of adipocyte hypertrophy and increased visceral adiposity. *Expert Rev Cardiovasc Ther* 2008; 6:343–368.

Am J Physiol Endocrinol Metab 298: E930–E940, 2010.
First published September 23, 2009; doi:10.1152/ajpendo.00320.2009.

Glucocorticoid reamplification within cells intensifies NF-κB and MAPK signaling and reinforces inflammation in activated preadipocytes

Takako Ishii-Yonemoto, Hiroaki Masuzaki, Shintaro Yasue, Sadanori Okada, Chisayo Kozuka, Tomohiro Tanaka, Michio Noguchi, Tsutomu Tomita, Junji Fujikura, Yuji Yamamoto, Ken Ebihara, Kiminori Hosoda, and Kazuwa Nakao

Division of Endocrinology and Metabolism, Department of Medicine and Clinical Science, Kyoto University Graduate School of Medicine, Sakyoku, Japan

Submitted 18 May 2009; accepted in final form 16 September 2009

Ishii-Yonemoto T, Masuzaki H, Yasue S, Okada S, Kozuka C, Tanaka T, Noguchi M, Tomita T, Fujikura J, Yamamoto Y, Ebihara K, Hosoda K, Nakao K. Glucocorticoid reamplification within cells intensifies NF-κB and MAPK signaling and reinforces inflammation in activated preadipocytes. *Am J Physiol Endocrinol Metab* 298: E930–E940, 2010. First published September 23, 2009; doi:10.1152/ajpendo.00320.2009.—Increased expression and activity of the intracellular glucocorticoid-reactivating enzyme 11β-hydroxysteroid dehydrogenase type 1 (11β-HSD1) contribute to dysfunction of adipose tissue. Although the pathophysiological role of 11β-HSD1 in mature adipocytes has long been investigated, its potential role in preadipocytes still remains obscure. The present study demonstrates that the expression of 11β-HSD1 in preadipocyte-rich stromal vascular fraction (SVF) cells in fat depots from *ob/ob* and diet-induced obese mice was markedly elevated compared with lean control. In 3T3-L1 preadipocytes, the level of mRNA and reductase activity of 11β-HSD1 was augmented by TNF-α, IL-1β, and LPS, with a concomitant increase in inducible nitric oxide synthase (iNOS), monocyte chemoattractant protein-1 (MCP-1), or IL-6 secretion. Pharmacological inhibition of 11β-HSD1 and RNA interference against 11β-HSD1 reduced the mRNA and protein levels of iNOS, MCP-1, and IL-6. In contrast, overexpression of 11β-HSD1 further augmented TNF-α-induced iNOS, IL-6, and MCP-1 expression. Moreover, 11β-HSD1 inhibitors attenuated TNF-α-induced phosphorylation of NF-κB p65 and p38-, JNK-, and ERK1/2-MAPK. Collectively, the present study provides novel evidence that inflammatory stimuli-induced 11β-HSD1 in activated preadipocytes intensifies NF-κB and MAPK signaling pathways and results in further induction of proinflammatory molecules. Not limited to 3T3-L1 preadipocytes, we also demonstrated that the notion was reproducible in the primary SVF cells from obese mice. These findings highlight an unexpected, proinflammatory role of reamplified glucocorticoids within preadipocytes in obese adipose tissue.

11β-hydroxysteroid dehydrogenase type 1; preadipocyte; nuclear factor-κB; mitogen-activated protein kinase; adipose inflammation

OBESE ADIPOSE TISSUE IS CHARACTERIZED by low-grade, chronic inflammation (24, 58). In humans and rodents, it has been shown that intracellular glucocorticoid reactivation is exaggerated in obese adipose tissue (38). Two isoenzymes, 11β-hydroxysteroid dehydrogenase type 1 (11β-HSD1) and type 2 (11β-HSD2), catalyze interconversion between hormonally active cortisol and inactive cortisone (2). In particular, 11β-HSD1 is abundantly expressed in adipose tissue and preferentially reactivates cortisol from cortisone (2). In contrast, 11β-HSD2 inactivates cortisol mainly in tissues involved in water and electrolyte metabolism (60). Transgenic mice overexpressing 11β-HSD1 in adipose tissue display a cluster of fuel dyshomeostasis (61). Conversely, systemic 11β-HSD1 knockouts and adipose-specific 11β-HSD2 overexpressors, which mimic adipose-specific 11β-HSD1 knockouts, are completely protected against diabetes and dyslipidemia on a high-fat diet (14, 30, 31, 42). Interestingly, 11β-HSD1 knockout mice on a high-fat diet showed preferential accumulation of subcutaneous adipose tissue, whereas wild-type mice accumulated considerable fat pads also in visceral (mesenteric) adipose tissue (39). These findings suggest that increased activity of 11β-HSD1 in adipose tissue contributes to dysfunction of adipose tissue and subsequent metabolic derangement.

Adipose tissue is composed of mature adipocytes (~50–70% of total cells), preadipocytes (~20–40%), macrophages (~1–30%), and other cell types (22). Biopsy studies of human adipose tissue demonstrated that the distribution of adipocyte diameter is bimodal, consisting of populations of very small adipocytes ("differentiating preadipocytes") and mature adipocytes (28, 35). Interestingly, the proportion of very small adipocytes was higher in obese people compared with the lean controls (28). Notably, insulin resistance was associated with an expanded population of small adipocytes and decreased expression of differentiation marker genes, suggesting that impairment of adipocyte differentiation may contribute to obesity-associated insulin resistance (35). In this context, a potential link between preadipocyte function and pathophysiology of obese adipose tissue has recently attracted research interest (53, 57).

Many of the genes overexpressed in mature adipocytes are associated with metabolic and secretory function, whereas the most representative function of the genes overexpressed in nonmature adipocytes, i.e., stromal vascular fraction (SVF) cells, is related to inflammation and immune response (9). Macrophage infiltration into obese adipose tissue contributes to local and systemic inflammation in subjects with obesity (63, 65). Furthermore, recent research (12, 48) highlights a pathophysiological role of preadipocytes in obese adipose tissue. In the proinflammatory milieu, preadipocytes act as macrophages (11, 13), share in phagocytic activities (11), and secrete an array of inflammatory substances (13).

A pharmacological dose of glucocorticoids is widely used for anti-inflammatory therapies in human clinics (49). On the other hand, recent research is highlighting the stimulatory effects of glucocorticoids on inflammatory response. Such effects are observed at lower concentrations relevant to phys-

Address for reprint requests and other correspondence: H. Masuzaki, Division of Endocrinology and Metabolism, Dept. of Medicine and Clinical Science, Kyoto University Graduate School of Medicine, 54, Shogoin Kawaharacho, Sakyoku, Kyoto, 606-8507, Japan (e-mail: hiroaki@kuhp.kyoto-u.ac.jp).

iological stress in vivo (35, 55, 66). Therefore, the potential role of 11β-HSD1 in a variety of inflammatory responses has stimulated academic interest (10, 26). Furthermore, it is known that mature adipocytes abundantly express 11β-HSD1, which is related to adipocyte dysfunction in obese adipose tissue (44, 61). On the other hand, the role of 11β-HSD1 in SVF cells remains largely unclear.

In this context, the present study was designed to explore the expression, regulation, and pathophysiological role of 11β-HSD1 in activated preadipocytes. The results demonstrate that inflammatory stimuli-induced 11β-HSD1 reinforces NF-κB and MAPK signals and results in induction of proinflammatory molecules.

MATERIALS AND METHODS

Reagents and chemicals. All reagents were of analytical grade unless otherwise indicated. TNF-α, IL-1β, LPS, and carbenoxolone (3, 52), a nonselective inhibitor for 11β-HSD1 and 11β-HSD2, were obtained from Sigma-Aldrich (St. Louis, MO). The recently developed 11β-HSD1 selective inhibitors 3-(1-adamantyl)-5,6,7,8,9,10-hexahydro[1,2,4]triazolo[4,3-α]azocine trifluoroacetate salt (WO03/065983, inhibitor A; Merck, Whitehouse Station, NJ; Ref. 23) and 2,4,6-trichloro-*N*-(5,5-dimethyl-7-oxo-4,5,6,7-tetrahydro-1,3-benzothiazol-2-yl) benzenesulfonamide (BVT-3498; Biovitrum, Stockholm, Sweden; Ref. 25) were synthesized according to the patent information.

Polyclonal antibodies against NF-κB p65, phospho-p65, p38 MAPK, phospho-p38, ERK1/2, phospho-ERK1/2, JNK, phospho-JNK, Akt, and phospho-Akt were purchased from Cell Signaling Technology (Beverly, MA). Polyclonal antibodies against SHIP1, PP2A, and MKP-1 were purchased from Santa Cruz Biotechnology (Santa Cruz, CA). An antibody against β-actin was purchased from Upstate Biotechnology (Lake Placid, NY). Horseradish peroxidase-conjugated anti-mouse, anti-rat, and anti-rabbit IgG antibodies and ECL Plus Western blotting detection kits were purchased from Amersham Biosciences (Piscataway, NJ).

Cell culture. 3T3-L1 cells (kindly provided by Dr. H. Green and Dr. M. Morikawa, Harvard Medical School, Boston, MA) were maintained in DMEM containing 10% (vol/vol) calf serum at 37°C under 10% CO_2.

Animals. Seventeen-week-old male C57BL/6 and nine-week-old *ob/ob* mice were used for the experiments. Mice were maintained on a standard diet (F-2, 3.7 kcal/g, 12% of kcal from fat, source soybean; Funahashi Farm) or a high-fat diet (Research Diets D12493, 5.2 kcal/g, 60% of kcal from fat, source soybean/lard) under a 14:10-h light-dark cycle at 23°C. The high-fat diet was administered to the diet-induced obese (DIO) mice from 3 to 17 wk of age. Animals were allowed free access to food and water. All animal experiments were undertaken in accordance with the guidelines for animal experiments of the Kyoto University Animal Research Committee.

Isolation of SVF and the mature adipocyte fraction. Subcutaneous (SQ), mesenteric (Mes), and epididymal (Epi) fat deposits were chopped using fine scissors and digested with 2 mg/ml collagenase (Type VIII; Sigma-Aldrich) in DMEM for 1 h at 37°C under continuous shaking (170 rpm). Dispersed tissue was filtered through a nylon mesh with a pore size of 250 μm and centrifuged. Digested material was separated by centrifugation at 1,800 rpm for 5 min. The sedimented SVF and cell supernatant [mature adipocyte fraction (MAF)] were both washed with DMEM. For primary culture experiments, SVF cells from epididymal fat pads were plated in sixwell plates and cultured overnight in DMEM containing 10% (vol/vol) FBS at 37°C under 10% CO_2. After being rinsed with the medium three times, the cells were incubated with or without TNF-α, carbenoxolone, or inhibitor A for 24 h.

Quantitative real-time PCR. Total RNA was extracted using Trizol reagent (Invitrogen, Carlsbad, CA), and cDNA was synthesized using an iScript cDNA synthesis kit (Bio-Rad, Hercules, CA) according to the manufacturer's instruction. The sequences of probes and primers are summarized in Suppl. Table S1 (supplemental data for this article are available at the *Am J Physiol Endocrinol Metab* website). Taqman PCR was performed using an ABI Prism 7300 sequence detection system following the manufacturer's instructions (Applied Biosystems, Foster City, CA). mRNA levels were normalized to those of 18S rRNA.

11β-HSD1 enzyme activity assay. 11β-HSD1 acts as a reductase and reactivates cortisol from cortisone in viable cells (54). In certain substrates, however, such as tissue homogenates or the microsome fraction, 11β-HSD1 acts as a dehydrogenase and inactivates cortisol to cortisone (8). 11β-HSD1 reductase activity in intact cells was measured as reported previously (8). Cells were incubated for 24 h in serum-free DMEM, with the addition of 250 nM cortisone and tritium-labeled tracer [1,2-^{3}H]$_2$-cortisone (Muromachi Yakuhin, Kyoto, Japan) for reductase activity and 250 nM cortisol with [1,2,6,7-^{3}H]$_4$-cortisol (Muromachi Yakuhin) for dehydrogenase activity. Cortisol and cortisone were extracted using ethyl acetate, evaporated, resuspended in ethanol, separated using thin-layer chromatography in 95:5 chloroform/methanol, and quantified using autoradiography.

To validate inhibitory potency of compounds against 11β-HSD1 with the use of FreeStyle 293 cells transiently transfected with human 11β-HSD1, the enzyme activity assay was carried out with 20 mM Tris · HCl at pH 7.0, 50 μM NADPH, 5 μg protein of microsomal fraction, and 300 nM [^{3}H]cortisone for 2 h. The reaction was stopped by 18β-glycyrrhetinic acid. The labeled cortisol product was captured by mouse monoclonal anti-cortisol antibody, bound to scintillation proximity assay beads coated with protein A, and quantified in a scintillation counter.

ELISA. Monocyte chemoattractant protein-1 (MCP-1) and IL-6 concentrations in the cultured media of 3T3-L1 preadipocytes were measured using ELISA according to the manufacturer's instructions (R&D Systems, Minneapolis, MN).

Western blot analysis. Two days after confluence, 3T3-L1 preadipocytes were stimulated with 10 ng/ml TNF-α in the absence or presence of 11β-HSD1 inhibitors (50 μM carbenoxolone or 10 μM inhibitor A) for 24 h.

For primary culture experiments, SVF from epididymal fat pads were plated in sixwell plates and cultured overnight in DMEM containing 10% (vol/vol) FBS at 37°C under 10% CO_2. After being rinsed with the medium three times, the cells were incubated with or without TNF-α, carbenoxolone, or inhibitor A for 24 h.

After 2-h serum starvation, cells were treated with TNF-α for 10 min to detect NF-κB and MAPK signals. Cells were washed with ice-cold PBS and harvested in lysis buffer (1% wt/vol SDS, 60 mM Tris · HCl, 1 mM Na_3VO_4, 0.1 mg/ml aprotinin, 1 mM PMSF, and 50 nM okadaic acid at pH 6.8) and boiled at 100°C for 10 min. After centrifugation, supernatants were normalized to the protein concentration via the Bradford method and then equal amounts of protein were subjected to SDS-PAGE and immunoblot analysis.

RNA interference. We tested four different small interfering RNA (siRNA) sequences. Stealth RNAi for mouse 11β-HSD1 (MSS205244, MSS205245, and MSS205246) (Invitrogen), and RNA interference (RNAi) for mouse 11β-HSD1 originally designed by an siRNA Design Support System (TaKaRa Bio, Shiga, Japan; sense: 5′-GAAAUGGCAUAUCAUCUGUTT-3′ and antisense: 3′-TTCUUUACCGUAUAGUAGACA-5′). MSS205245 and MSS205246 did not suppress the 11β-HSD1 mRNA level effectively in preliminary experiments. Therefore, we demonstrated the data of MSS205244 [si(1)] and of the originally designed siRNA [si(2)] in this study. According to the manufacturer's protocol, 3T3-L1 preadipocytes were transfected with 10 nM siRNA in antibiotic-free medium using Lipofectamine RNAiMAX (Invitrogen). We assessed the ransfection efficiency using green fluorescent protein (GFP) detection (pmaxGFP), according to the manufacturer's instructions (Amaxa, Cologne, Germany). Fluorescent microscopic observa-

tion revealed that more than two-thirds of the cells expressed GFP (data not shown).

Expression vector. A mammalian expression vector encoding Hsd11b1 (Hsd11b1/pcDNA3.1) was constructed by inserting cDNA for mouse 11β-HSD1 into pcDNA3.1 (Invitrogen). 3T3-L1 preadipocytes were detached from culture dishes using 0.25% trypsin. Cells (5×10^6) were mixed with 2 μg plasmid in the solution provided with the cell line Nucleofector Kit V (Amaxa). pcDNA3.1/11β-HSD1 or a control vector was introduced into the cells using electroporation with a Nucleofector (Amaxa) instrument according to the manufacturer's instructions.

Statistical analysis. Data are expressed as the means ± SE of triplicate experiments. Data were analyzed using one-way ANOVA, followed by Student's *t*-tests for each pair of multiple comparisons. Differences were considered significant if $P < 0.05$.

RESULTS

Expression of 11β-HSD1 was elevated in the MAF and in SVF isolated from fat depots in ob/ob mice and DIO mice. Genetic (*ob/ob*) and dietary (DIO) obese models were analyzed. Expression of iNOS, MCP-1, and IL-6, all of which are obesity-related proinflammatory mediators (19, 29, 45, 56), was elevated in the MAF and SVF from both *ob/ob* mice and DIO mice compared with lean littermates (Fig. 1, *A* and *B*). Levels of 11β-HSD1 mRNA in the MAF from obese mice were substantially elevated compared with their lean littermates (*ob/ob*: SQ, 5-fold; Mes, 62-fold) (DIO: SQ, 24-fold; Mes, 460-fold; Fig. 1, *A* and *B*). On the other hand, levels of 11β-HSD1 mRNA in SVF from *ob/ob* mice and DIO mice were also elevated compared with their lean littermates (*ob/ob*: SQ, 3-fold; Mes, 3-fold; and DIO: SQ, 8-fold, Mes, 4-fold; Fig. 1, *A* and *B*).

TNF-α, IL-1β, and LPS augmented 11β-HSD1 mRNA expression and reductase activity in 3T3-L1 preadipocytes. When 3T3-L1 preadipocytes were treated with TNF-α (10 ng/ml) for 24 h, mRNA levels of 11β-HSD1 markedly increased (~4-fold; Fig. 2*iv*). Levels of iNOS, MCP-1, and IL-6 mRNA were concomitantly increased (50-, 70-, and 200-fold, respectively; Fig. 2, *i–iii*). IL-1β (1 ng/ml) and LPS (1,000 ng/ml) substantially augmented 11β-HSD1 mRNA expression in 3T3-L1 preadipocytes (10- and 3-fold vs. control, respectively) (Fig. 2*iv*). Reductase activity of 11β-HSD1 was augmented by TNF-α, IL-1β, and LPS compared with the control (2-, 9-, and 6-fold vs. control, respectively; $P < 0.05$; Fig. 2*v*). Based on the results of 11β-HSD1 activity, TNF-α was used at 10 ng/ml in subsequent experiments. On the other hand, 11β-HSD2 mRNA and the corresponding dehydrogenase activity were undetected not only at the baseline condition but with TNF-α, IL-1β, and LPS treatments (data not shown).

Dexamethasone decreased iNOS, MCP-1, and IL-6 mRNA and protein levels in TNF-α-treated 3T3-L1 preadipocytes. The effects of glucocorticoid on proinflammatory gene expression in TNF-α-treated 3T3-L1 preadipocytes were examined over a wide range of concentrations (10^{-10}, 10^{-9}, 10^{-8}, and 10^{-7} M), representing physiological to therapeutical levels in vivo (5). Dexamethasone (10^{-7} M) decreased mRNA levels of iNOS, MCP-1, and IL-6 (iNOS: 85 ± 2%, MCP-1: 40 ± 16%, and IL-6: 97 ± 1% reduction vs. TNF-α-treated cells) and protein levels in the media (MCP-1: 48 ± 5% and IL-6: 83 ± 1% reduction) in TNF-α-treated 3T3-L1 preadipocytes (Suppl. Fig. S1).

Pharmacological inhibition of 11β-HSD1 attenuated iNOS, MCP-1, and IL-6 mRNA and protein levels in TNF-α-treated 3T3-L1 preadipocytes. The effects of pharmacological inhibition of 11β-HSD1 on proinflammatory gene expression were examined in TNFα-treated 3T3-L1 preadipocytes. In previous in vitro studies, carbenoxolone (CBX), a nonselective inhibitor of 11β-HSD1 and 11β-HSD2, was used at concentrations from 5 to 300 μM (16, 17, 26). To date, an 11β-HSD1-specific

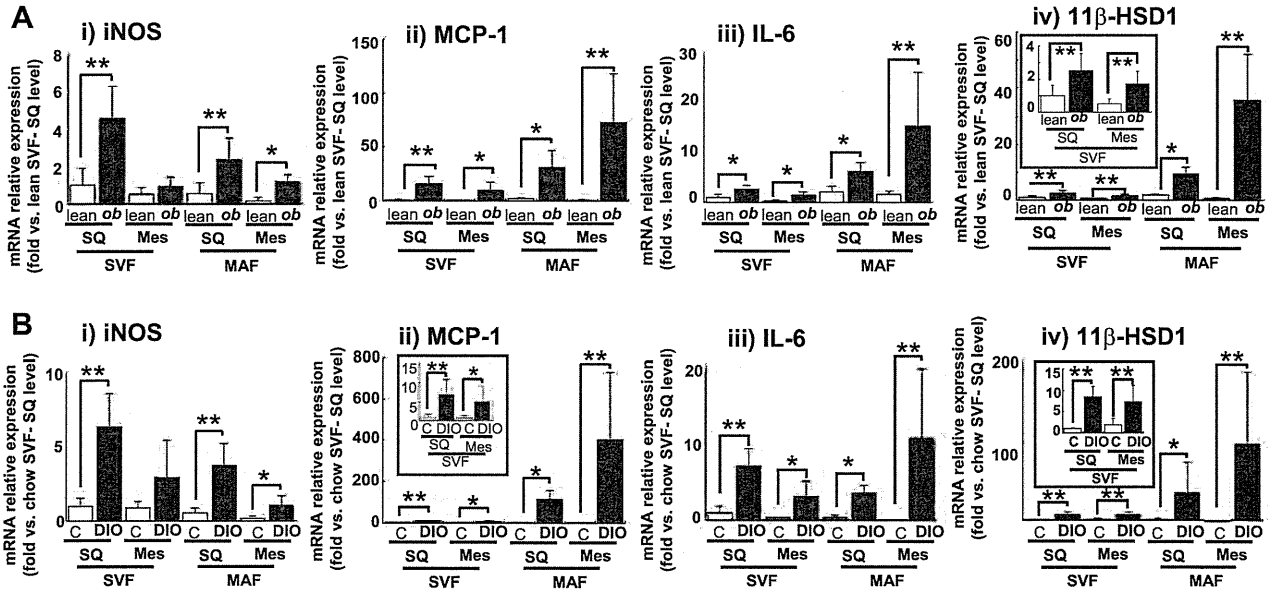

Fig. 1. 11β-Hydroxysteroid dehydrogenase type 1 (11β-HSD1) mRNA expression in stromal vascular fraction cells (SVF) and mature adipocytes fraction (MAF) isolated from obese adipose tissue of *ob/ob* mice and diet-induced obese (DIO) mice. *A*: *ob/ob* and lean littermates [control (C) 9 wk of age; $n = 6$]. *B*: DIO and littermates on a chow diet (17 wk of age; $n = 6$). Levels of inducible nitric oxide synthase (iNOS; *i*), monocyte chemoattractant protein-1 (MCP-1; *ii*), IL-6 (*iii*), and 11β-HSD1 (*iv*) mRNA in SVF and MAF in subcutaneous abdominal fat depots (SQ) and mesenteric fat depots (Mes). *$P < 0.05$, **$P < 0.01$ compared with lean littermates.

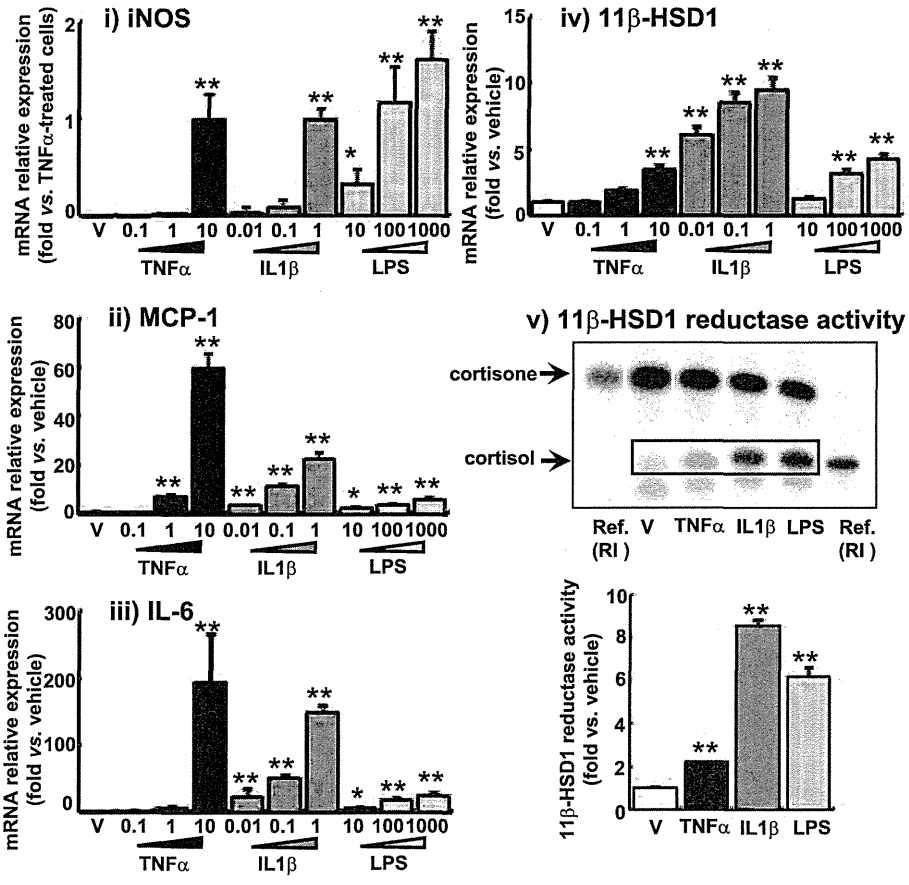

Fig. 2. TNF-α, IL-1β, and LPS augment the expression of proinflammatory mediators and 11β-HSD1 in 3T3-L1 preadipocytes. Cells were treated with TNF-α (0.1, 1, and 10 ng/ml), IL-1β, (0.01, 0.1, and 1 ng/ml) or LPS (10, 100, and 1,000 ng/ml) for 24 h. Levels of iNOS (*i*), MCP-1 (*ii*), IL-6 (*iii*), and 11β-HSD1 (*iv*) mRNA were quantified using real-time PCR. Values were normalized to that of 18S rRNA. *v*: 11β-HSD1 reductase activity (expressed as conversion ability of cortisone to cortisol) was assessed in the medium of 3T3-L1 cells treated with 10 ng/ml TNF-α, 1 ng/ml IL-1β, or 1,000 ng/ml LPS for 24 h. A reference of [^{3}H]cortisone or [^{3}H]cortisol was used as a size marker. A representative autoradiograph of thin-layer chromatography in 11β-HSD reductase activity assay (*top*) and quantification (*bottom*). Intensities of cortisol signals correspond to the enzyme activity of reductase. Ref. (RI), reference samples of [^{3}H]cortisone or [^{3}H]cortisol as size marker. Data are means ± SE of triplicate experiments. $^*P < 0.05$, $^{**}P < 0.01$, compared with vehicle (V)-treated group.

inhibitor, inhibitor A, has not been used for in vitro studies; however, another 11β-HSD1-specific inhibitor (compound 544) sharing almost the same structure as inhibitor A was used at a concentration of 5 μM (62). Therefore, in the present study, 10–50 μM CBX and 2.5–10 μM inhibitor A were used.

Before using these inhibitors in intact cells, we validated inhibitory potency of compounds against 11β-HSD1 in the microsome fraction assay. We verified that inhibitor A (10 nM) and CBX (1 μM) inhibited 11β-HSD1 activity as little as 25% vs. control, respectively, and that both of the 11β-HSD inhibitors suppressed 11β-HSD activity in a dose-dependent manner (Suppl. Fig. S2).

In 3T3-L1 preadipocytes, although CBX and inhibitor A did not change the level of 11β-HSD1 reductase activity, both of them suppressed TNF-α-induced reductase activity of 11β-HSD1 in a dose-dependent manner (Fig. 3*A*). CBX (50 μM) and inhibitor A (10 μM) markedly attenuated 11β-HSD1 activity (78 and 60% reduction vs. TNF-α-treated cells, respectively; Fig. 3*A*).

Without TNF-α-treatment, CBX and inhibitor A did not affect mRNA or protein levels of iNOS, MCP-1, and IL-6. On the other hand, in TNF-α-treated cells, these inhibitors reduced the mRNA and protein levels of proinflammatory genes. CBX decreased iNOS, MCP-1, and IL-6 mRNA levels (50 μM; iNOS: 83 ± 5%, MCP-1: 27 ± 4%, and IL-6: 47 ± 10% reduction vs. TNF-α-treated cells without compounds) and protein levels in the media (MCP-1: 17 ± 1% and IL-6: 34 ± 6% reduction) in TNF-α-treated 3T3-L1 preadipocytes (Fig. 3*B*). Similarly, inhibitor A reduced iNOS, MCP-1, and IL-6 mRNA (10 μM; iNOS: 47 ± 13%, MCP-1: 32 ± 12%, and IL-6: 33 ± 9% reduction) and protein levels in the media (MCP-1: 47 ± 3% and IL-6: 14 ± 3% reduction) (Fig. 3*C*).

Effect of 11β-HSD1 knockdown on proinflammatory properties in 3T3-L1 preadipocytes. To explore the potential role of 11β-HSD1 in cytokine release from activated preadipocytes, 11β-HSD1 was knocked down using siRNA. We tested four different siRNA sequences as described in MATERIALS AND METHODS; however, two of them did not suppress 11β-HSD1 mRNA level significantly in the preliminary experiments. Thus we demonstrated the data on si(1) and si(2).

When 3T3-L1 preadipocytes were transfected with 11β-HSD1 siRNA, TNF-α-induced expression of 11β-HSD1 was markedly attenuated [si(1): 60 ± 9% and si(2): 88 ± 7% reduction vs. negative control siRNA; Fig. 4*A*, *i*]. 11β-HSD1 reductase activity was also decreased by 11β-HSD1 siRNA [si(1): 81 ± 9% and si(2): 84 ± 3% reduction vs. negative control siRNA; Fig. 4*A*, *ii*]. 11β-HSD2 mRNA levels and the corresponding dehydrogenase activity were under detectable with or without siRNA treatments in 3T3-L1 preadipocytes (data not sown). Negative control RNAi did not influence the expression of 11β-HSD1. Knockdown of 11β-HSD1 in TNF-α-treated 3T3-L1 preadipocytes effectively reduced iNOS, MCP-1, and IL-6 mRNA levels [si(1): IL-6: 32 ± 7% reduction; and si(2): iNOS: 37 ± 8%, MCP-1: 22 ± 5%, and IL-6: 59 ± 3% reduction] and protein levels in the media [si(1):